Theoretical Studies of Structures of Compressed Hydrogen

— Vibrational frequencies at the Γ-point and Evaluation of the zero-point energy with its effect on the transition pressures —

Tomoki TAKEZAWA

OSAKA UNIVERSITY
GRADUATE SCHOOL OF ENGINEERING SCIENCE
DEPARTMENT OF PHYSICAL SCIENCE
DIVISION OF MATERIALS PHYSICS

1999

Abstract

Structures of highly compressed hydrogen are studied through first principles calculations of the total energy, vibrational frequencies and the zero-point motion energy of the nuclei. The band theoretical approach using plane-wave basis functions is employed with the local density approximation to the exchange-correlation energy. The electronic states are calculated by the iterative scheme using conjugate gradient method to save the machine time and memory. In the calculations of the effective force constants among atoms, the supercell method which gives exact frequencies at several points in the Brillouin zone and the Hellman-Feynman theorem are used.

For structures newly proposed by experimental and theoretical studies of the molecular phase, vibrational optical-mode frequencies have been calculated in the harmonic approximation and compared with experimental values obtained by recent Raman scattering and infrared (IR) absorption experiments. Special attention is payed to the $Pa3$ structure whose possibility is pointed out by very recent study of the Raman measurement and to the $Cmca$ structure which has been predicted to be one of low energy structures and also suggested in the same Raman experiment.

The optical-mode frequencies in the $Pa3$ structure is compatible with the frequencies obtained by the Raman and IR experiments in the phase II but the pressure dependencies of the frequencies show some discrepancies in the phase III. The frequencies in the $Cmca$ structure are incompatible at pressures lower than $\sim$ 200 GPa.

For most probable structures theoretically proposed for the atomic phase and that for the molecular phase, the phonon frequencies are calculated in the harmonic approximation at several points in the Brillouin zone. From the

phonon frequencies over the Brillouin zone, the stabilities of the structures are studied. The zero-point energies of the proton motions are also evaluated and the effects on the pressures, especially on the pressure of molecular dissociation, are studied.

The $Cs-IV$ structure is stable in the atomic phase. The $Cmca$ structure of the molecular phase has weakly unstable modes, which are studied in detail. The zero-point energies calculated for these two structures by present harmonic treatments are compared with those of former studies including quantum Monte Carlo study. Our zero-point energies are close to those obtained for other structures by perturbational methods but are about a half of those estimated by quantum Monte Carlo calculations. With effect of the zero-point energy, the dissociation pressure is decreased by about 60 GPa owing to the larger zero-point energy in the molecular phase than that in the atomic phase. The decrease of the transition pressure means that the transition pressure is lower for hydrogen than for the deuterium.

According to the present study, the most probable structures in the molecular phase at pressures lower than 200 GPa are the $Pca2_1$ or the $Cmc2_1$ structure. The $Cmc2_1$ structure persists above 200 GPa. As the pressure is further increased, the structure of the $Cmc2_1$ becomes close to the that of the $Cmca$. The molecular phase persists up to $\sim$ 400 GPa and the phase possibly become metallic before the molecular dissociation. The $Cs-IV$ structure is probable after the molecular dissociation.

ACKNOWLEDGMENTS

The author would like to express his sincere thanks to Dr. Hitose Nagara for introducing him to the subjects and helpful discussions. He also wishes to thank Prof. Hiroshi Miyagi for valuable discussions and Dr. Kazutaka Nagao for kind instructions and valuable discussions. Thanks are also due to the other members of Miyagi laboratory.

Contents

I. INTRODUCTION

Since Wigner and Huntington's pioneering work predicting the pressure induced molecular dissociation of hydrogen molecules and its resulting metallic state [1], the metallic hydrogen has attracted numbers of physicists for more than sixty years. The original scenario of the metallization proposed by Wigner and Huntington is that, after the molecular dissociation, the hydrogen atoms each of which has one electron form the half-filled electronic band, like alkaline metals. And later, another scenario of metallization has been proposed that the electronic bands formed by the hydrogen molecules, which are the filled bands at low densities, become overlapped at high densities and form partially filled electronic bands [2,3]. Both scenarios have been widely studied in experimental as well as theoretical studies. Possibility of the high temperature superconductivity has added further interests to this substance [4–7] and has been intensively studied in both molecular and atomic phases [8,9].

Metallic hydrogen has long been a substance of astrophysical interests related to the interior structure of giant planets [10]. However, owing to recent advancement in high pressure techniques at laboratories the substance of celestial interests has changed into a target of experimental challenge in the laboratories [11,12]. The static compression methods using diamond anvil cells [13], as well as shock-compression [12] ones, are widely used in recent high pressure experiments. Most remarkable results in recent shock-compression experiments [12] on the liquid hydrogen and deuterium are sharp decrease in the resistivity (Fig.1), by about four orders of magnitude, observed around 140 GPa (100 GPa = 1 Mbar) at relatively low temperature of few thousands degrees. Similar experiments reported also the significant deviation of the compressibility of liquid deuterium from that of the former theoretical prediction (Fig.2), which suggests the increased molecular dissociation at elevated temperatures [14]. These results may affect the understanding of the interior structure of the giant planets [15].

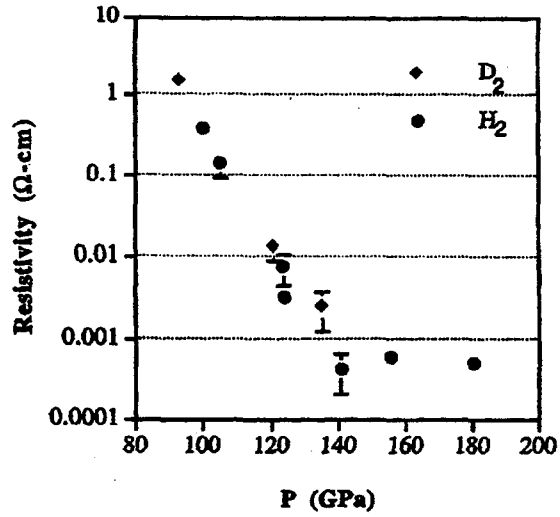

FIG. 1. Pressure dependence of the resistivity. (From Ref. [12])

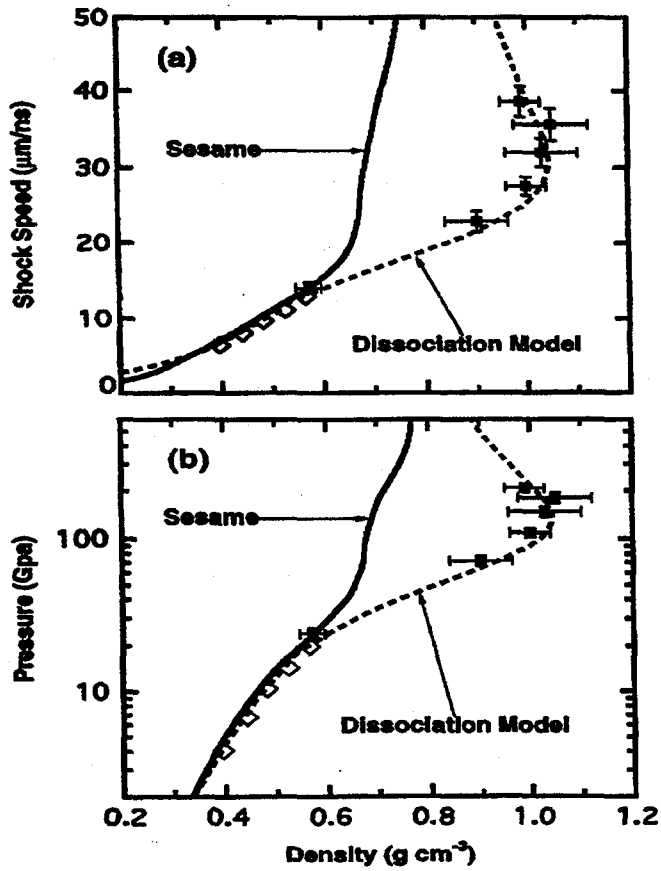

FIG. 2. Deviation of the compressibility of liquid deuterium from that of the former theoretical prediction. The Sesame is the EOS by G. I. Kerley, Los Alamos Science Laboratory Report No. LA-4776, 1972. (From Ref. [14])

In the meantime the static compression experiments on the hydrogen and deuterium using diamond anvil cell have been performed at room and lower temperatures up to $\sim$ 250 GPa [16,17]. The first evidence of the phase transition at megabar pressures is the sudden drop of the vibron frequencies at around 150 GPa(Fig.3). The pressures at which the drop occurs are nearly same for hydrogen and for deuterium, which has been mysterious from the point of view of largest mass effects expected in this substance. Although the nature of this transition is still not clear, the subsequent experiments revealed new important experimental data [11,16–24] for the determination of the phase diagram. The phase boundaries among three phases in the solid hydrogen and deuterium have been established experimentally [11,20] (Fig.4), and the lattice of the molecular centers has been determined at room temperature to be hcp up to $\sim$ 120 GPa by the X-ray experiment [18]. The phase diagram of deuterium determined by recent experiments is given in Fig.5. Recent Raman experiment [23] also has reported possibility of further rich phase diagram in the ortho-para [25] mixed crystals. However, no evidence of the metallization nor the molecular dissociation has been confirmed so far.

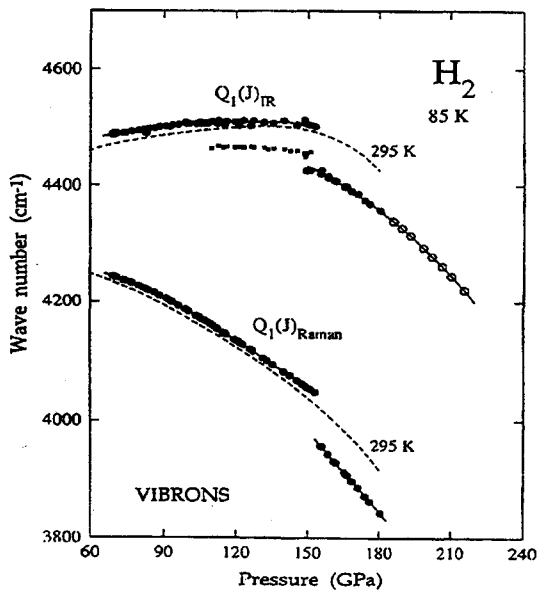

FIG. 3. The vibron drops around 150 GPa (From Ref. [11])

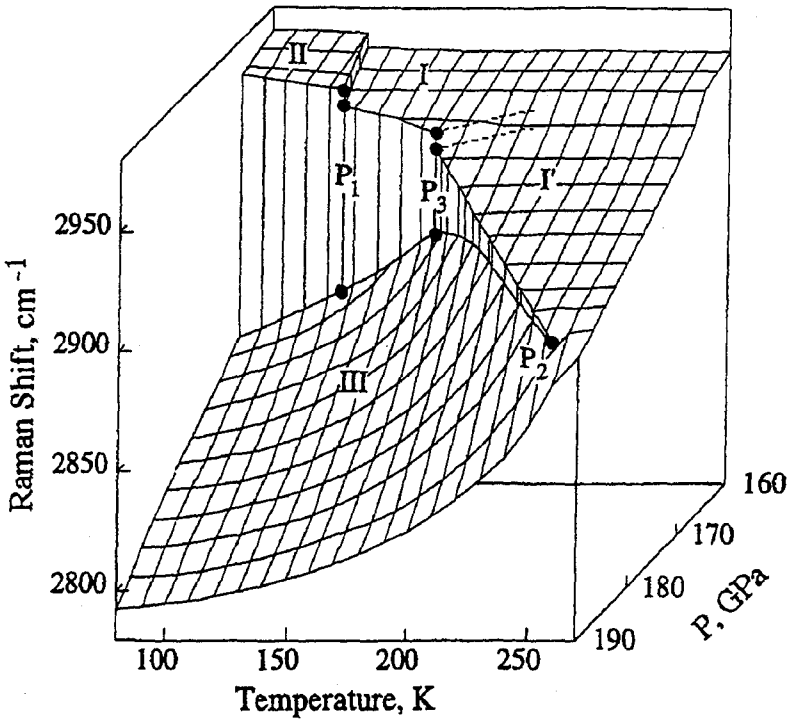

FIG. 4. The Raman frequency shifts for the determination of phase boundaries of deuterium. (From Ref. [22])

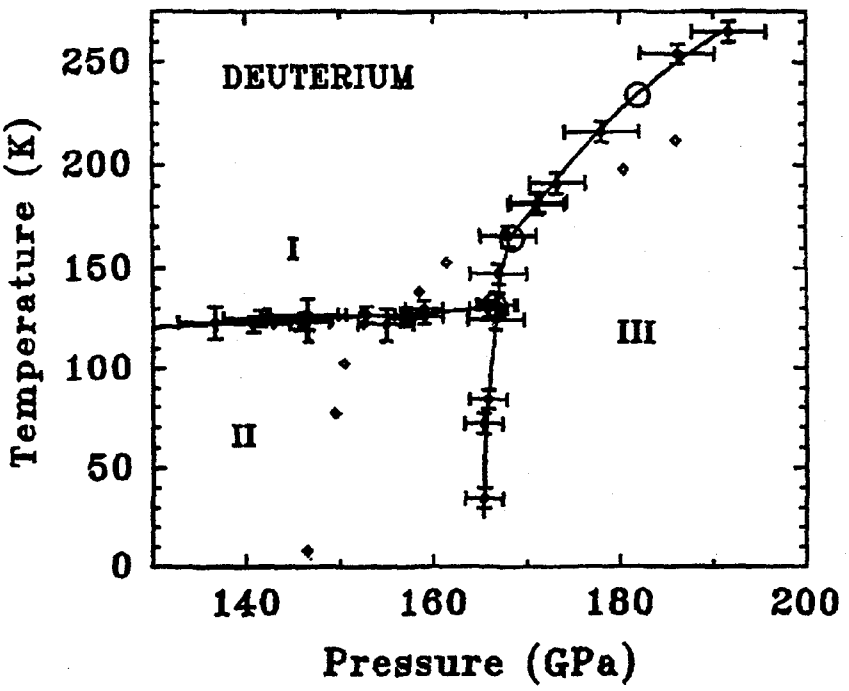

FIG. 5. The phase diagram of deuterium. (From Ref. [22])

In the theoretical side, number of theoretical predictions of the molecular dissociation and the metallization in compressed hydrogen have appeared. The predicted pressures, however, are widely scattered: the pressure of the metalization ranges over the region of 1 $\sim$ 3 Mbar and that of the dissociation over 3 $\sim$ 6 Mbar [26–31]. The theoretical studies can not, so far, predict which of the scenarios, the metallization by the molecular dissociation or the metallization by the overlapping of the molecular orbital bands, occurs first at high pressures. One of the main reasons for the difficulty in the predictions may be the quantum effects [32–35] expected in this lightest element under condition of lacking the information of the structures at megabar pressures. The crystal structures in both molecular and atomic phases are essential to the prediction of the pressure of the band overlapping in the molecular phase or the molecular dissociation, at low temperatures.

In this thesis, we study structures of compressed hydrogen through *ab initio* calculations of the total energy and vibrational frequencies based on the local density approximation (LDA) and partly on the generalized gradient approximation (GGA) for the exchange correlation energy. We calculate the vibrational frequencies at several points in the Brillouin zone. From the frequencies and modes, we discuss the stabilities of the structures at high pressures. We evaluate also the zero-point energy and its effects on the transition pressures.

Following introduction, in section II, we study the total energies of the structures predicted in earlier studies for both atomic and molecular phases as well as those of newly proposed structures to pick out the candidate structures. In section III, we study frequencies of the IR and Raman active vibrational modes in the molecular phase at megabar pressures. In section IV, we study the dispersion of the vibrational frequencies over the Brillouin zone through the first principle LDA band theoretical treatments and discuss the stability of the structures. We also calculate the zero-point energy and evaluate its effects on the pressure of molecular dissociation. In section V, we discuss the probable structures of hydrogen at megabar pressures. Conclusions and some remarks follow in the last section.

II. TO SINGLE OUT CANDIDATE STRUCTURES IN EACH PHASE

Owing to extremely wide range of the density interested, the study of compressed hydrogen requires appropriate method for each density region and various approaches have been developed. In the first study of the metallic hydrogen, Wigner and Huntington used the cellular method to obtain the electronic bands and the total energy [1]. They predicted that the metallization needs around 25 GPa in the most advantageous case. Later the many-body perturbational approaches were widely used in the calculation of total energy [36–38] for numbers of structures. The results by perturbational approaches are exact at high density limit. However, as the density is decreased the higher order terms become important, and the accuracy is decreased by the ambiguity of contributions from higher order terms. As computer resources increase, the Hartree-Fock and other band theoretical approaches for the total energy calculations appeared [2] and used for some structures in the atomic as well as the molecular phase.

Min, Jansen, and Freeman [39] is the first who employed density functional approach in the full potential augmented-plane-wave band calculation for the total energy of compressed hydrogen. They studied cubic structures in the atomic phase and $Pa3$ structure in the molecular phase. Following Min *et al.*'s study many calculations started in search for stable structures in both atomic and molecular phases. In most recent theoretical studies of the compressed hydrogen, the local density approximation (LDA) to the exchange-correlation energy is widely used in the calculation of the electronic bands along with the plane wave (PW) basis function to reduce the inaccuracy of the energy difference among structures [40]. Numbers of theoretical studies [26,30] in the LDA with use of the PW have been carried out including molecular dynamics study [41].

We will single out, in the following subsections, the structures in the atomic phase as well as those in the molecular phase from the structures proposed by experimental and theoretical works on hydrogen and deuterium at megabar and higher pressures.

A. Atomic Phase

At the extreme limit of pressure, the assembly of atoms looks like the point charges immersed in the uniform neutralizing charge background, which is the classical one component plasma (OCP) [42] widely studied by the plasma- and astro-physicists. The energy of the OCP at T=0, which is identical to the Madelung energy of solid, was extensively studied theoretically and the energy is lower for the lattice of higher coordination like bcc, fcc, hcp etc. The bcc structure is known to be of lowest energy and all matters take the bcc structure at this extreme pressure of celestial interests.

As the density is decreased, the screening effects of the electrons on the nuclear charge become important. Brovman *et al.* [36] studied the structures in the atomic phase by the use of many-body perturbational expansion starting from the system of the protons immersed in the uniform electron gas. They predicted the possibility of the structure of low coordination, like two-dimensional (planar) structures and one-dimensional (filamentary) ones.

This possibility was supported by the LDA calculations carried out later [26,43](Fig.6). The low dimensional anisotropic structures, however, are studied again by the QMC calculations and the energy of the anisotropic structure becomes higher than the diamond structure when the contribution of the zero-point energy [34] is taken into account. Very recently Nagao and Nagara studied the family of tetragonal diamond structures (Fig.7) and point out the possible instability of the cubic diamond structure [31](Fig.8).

According to the total energy calculation in the clamped nuclei approximation carried out so far, the candidate structures in the atomic phase into which the structure in the molecular phase may transforms are the $Cs-IV$ or the $\beta-Sn$ structure. We will study, in section IV, the zero-point energy of the proton motion in these structures and its effects.

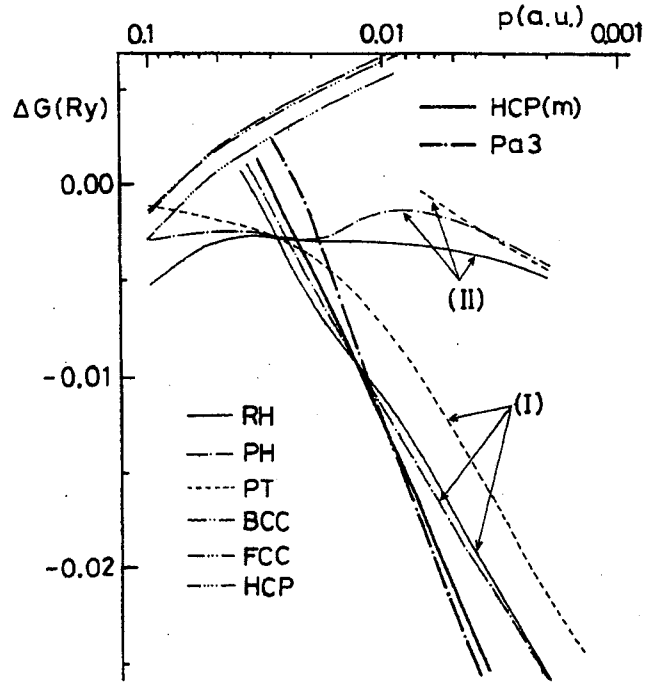

FIG. 6. Free energy difference among structures. (From Ref. [43])

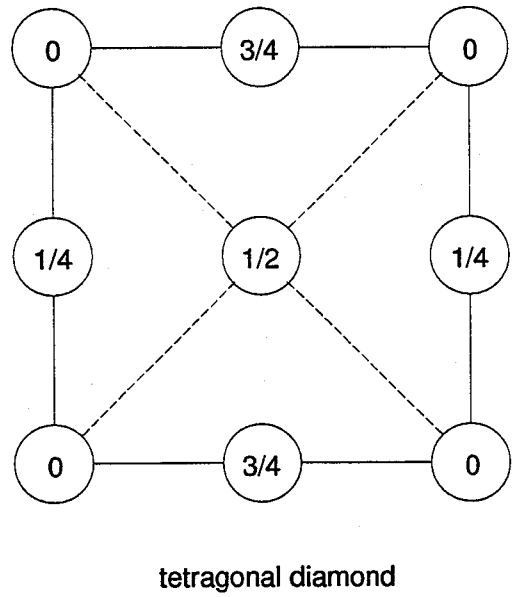

FIG. 7. The tetragonal diamond structure. The numbers in the circles denote the heights of atoms. The $Cs-IV$,$\beta-Sn$ and diamond structures are characterized by the $c/a > \sqrt{2}$, $c/a < \sqrt{2}$ and $c/a = \sqrt{2}$ respectively.

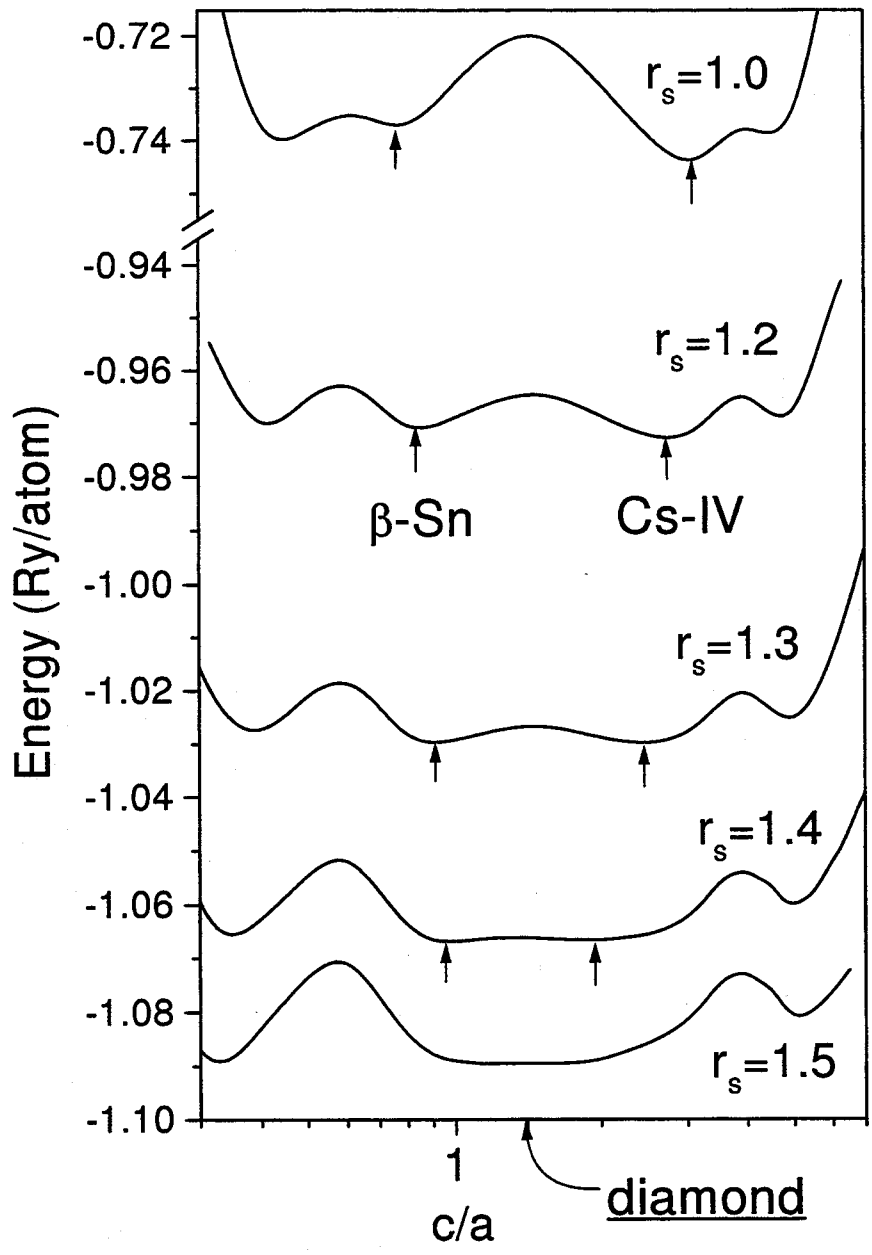

FIG. 8. Energy as functions of c/a at some densities in the tetragonal diamond family. (From Ref. [31])

B. Molecular Phase

At ambient pressure, hydrogen liquefies at temperature 20 K and as temperature is reduced further it becomes solid at 14 K in which hydrogen molecules form a crystal lattice. At pressure higher than about 5 GPa, the melting point of the solid exceeds room temperature. The solid which consists of the ortho-species of the hydrogen has the orientationally ordered structure with space group $Pa3$ at sufficiently low temperature, in which the molecular centers sit on the fcc sites. As the temperature is raised the orientational order is destroyed and the fcc lattice of the molecular center transforms into the hcp lattice. The solid of the para-species of hydrogen which is orientationally isotropic forms hcp lattice of the molecular centers at all temperatures.

Experimental determination of the structures of hydrogen by the X-ray diffraction faced great difficulty of low intensity under high pressure due to extremely small sample size in diamond anvil cells and low X-ray scattering efficiency of the hydrogen atom. The lattice of the molecular centers was determined to be hcp by Hazen *et al.* [44] at 5.4 GPa and at room temperature using single crystal and then the hcp structure was confirmed up to 26.5 GPa by the experiment using synchrotron source of X-ray [45]. Very recently Loubeyer *et al.* have confirmed the hcp lattice up to 120 GPa at room temperature [18].

The possibility of pressure induced molecular orientation have long been interested in the crystal of para-hydrogen molecules which are in quantum mechanically spherical states and the first report on the experimental evidence of the probable orientational order was published by Silvera *et al.* [46] in ortho-deuterium at about 28 GPa and later by Lorenzana *et al.* [47] at around 110 GPa in para-hydrogen. The point of those phase transitions are shown in Fig.9.

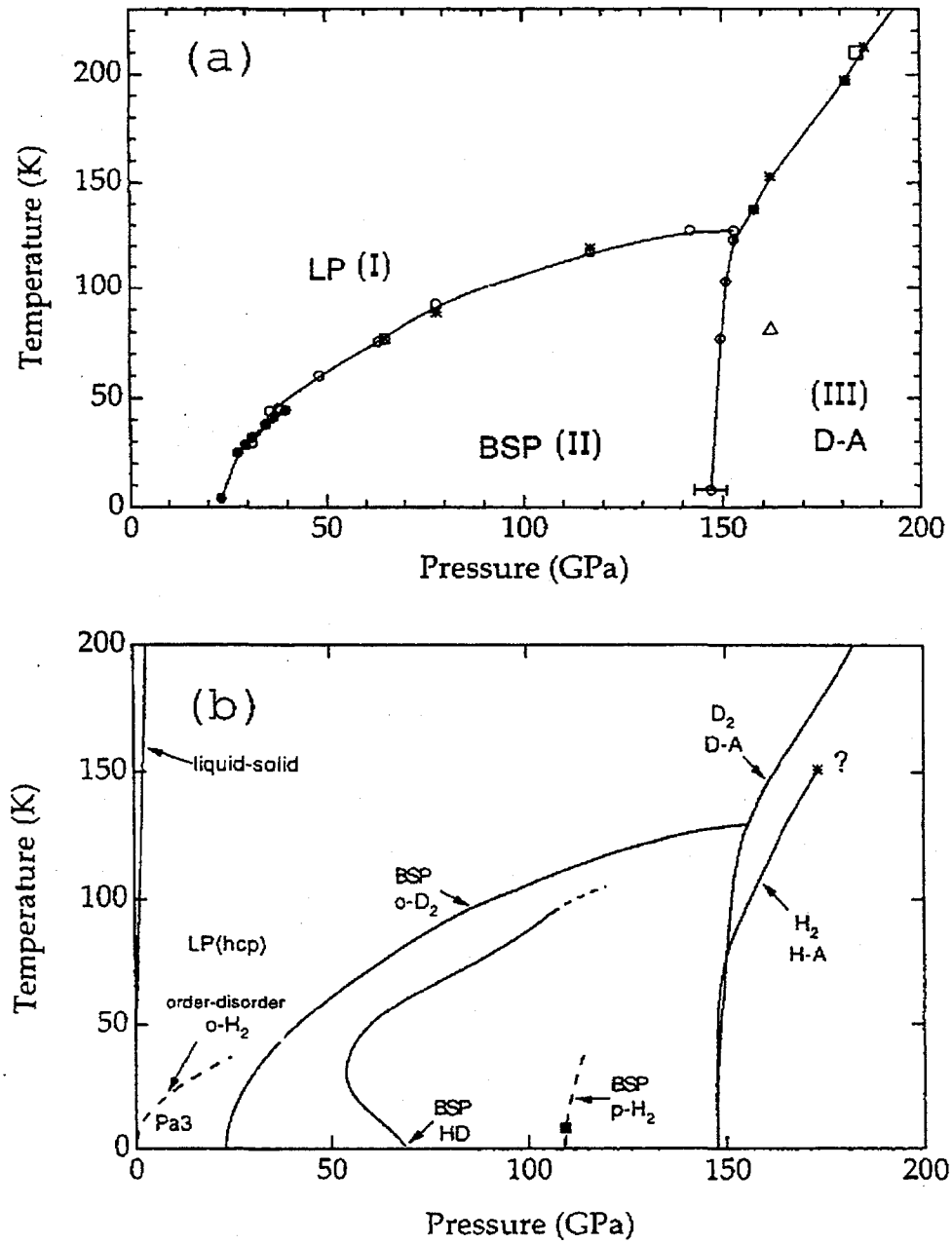

FIG. 9. Difference of the phase boundary between hydrogen and deuterium. (From Ref. [20])

From the pressure dependences of the Raman peaks [48] at room temperature the hcp lattice of the molecular centers are thought to persists to around 150 GPa. The lattice of the molecular centers at low temperatures are unclear relating to the molecular orientations. The

available experimental data on the molecular orientations in the solid hydrogen at megabar pressures are those from Raman and Infrared experiments [21].

Along with the experimental studies, many theoretical studies are now being carried out by the use of band theoretical approaches [31], molecular dynamics [41] and path integral approach [49]. The probable structures proposed by experimental and theoretical studies are: in phase I, the molecular centers are on the hcp lattice as is determined by the X-ray experiments and the molecules are rotating, in phase II the molecules are oriented to some pattern of orientational order or of partial order, and in phase III molecules are oriented in a pattern of order nearly like classical orientation. However more intensive studies are needed to establish the structures in phase II and III. The proposed orientational patterns of the molecular orientation in phase II and III are given in Fig.10.

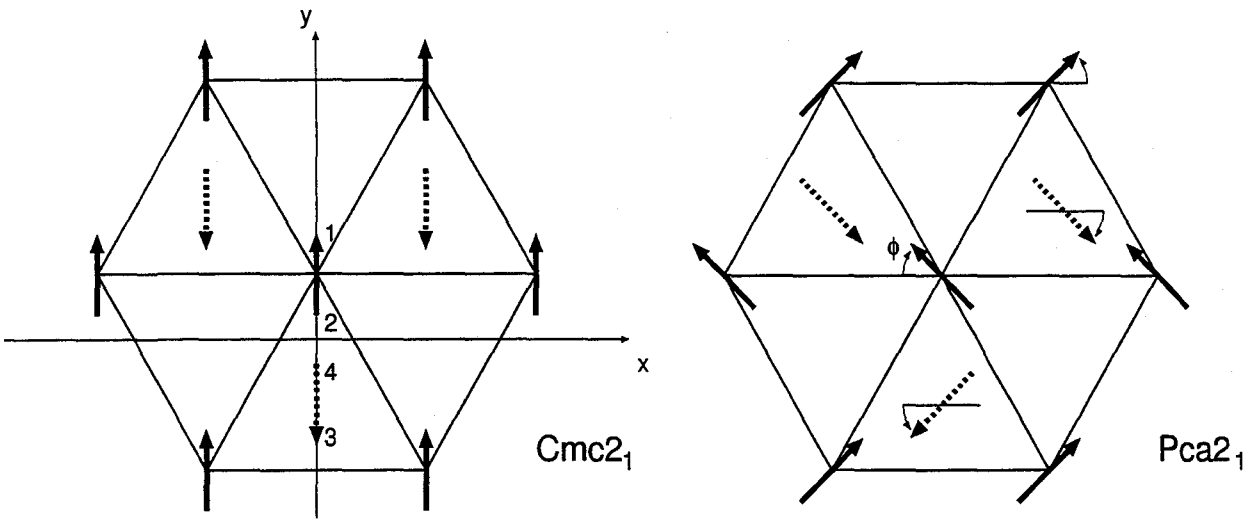

FIG. 10. Proposed orientational patterns of the molecule in the molecular phase.(From Ref. [50]) Solid lines represent molecules lying in a c-plane and broken ones in the next c-plane. Arrows indicate the direction of molecular axes whose direction cosines with the z-axes are positive.

Among those patterns of molecular orientations in the hcp lattice, the total energy calculation in the LDA and in the clamped nuclei approximation, in which the protons

are fixed at the position assumed at the beginning of the calculation of electronic states, predicts that the $Pca2_1$ is of lowest energy up to around 200 GPa. The $Cmc2_1$ structure which corresponds to the particular orientation of the molecule in the $Pca2_1$ has the total energy very close to the $Pca2_1$.

Besides the hcp lattice of the molecular centers, possibility of the fcc lattice has been proposed from experimental study, which will be studied below in detail in section III.

C. Structure above 200 GPa in the Molecular Phase

At pressures near 200 GPa, possibility of the deviation of molecular centers from the sites of the hcp lattice has been pointed out theoretically [51,41]. The $Cmc2_1$ structure permits, without changing the space group, the displacements of one of the molecular centers of the hcp lattice towards the site of the $Cmca$ structure which is given in Fig.11. We observe a series of structural changes from the $Pca2_1$ to the $Cmca$ structure. The $Pca2_1$ structure changes into the $Cmc2_1$ structure at the special value of the azimuthal angle $\phi = 90°$ as shown in Fig.10. With the above displacement of the molecular center, the $Cmc2_1$ structure transforms into the $Cmca$ at some value of the displacement, which can be seen in Fig.11.

We study the total energy of the $Cmc2_1$ structure in the GGA as a function of the displacement. The results are shown in Fig.12 where the molecular orientations are fixed in the calculation. At pressures around 150 GPa, the displacement of the molecular center from the hcp sites are small but as the pressure is increased the deviation becomes large and around 200 GPa the molecular centers reach to those of the $Cmca$ structure. The pressure dependence of the enthalpy is plotted in Fig.13 taking the diamond structure of atomic phase as a reference and compared with those of other structures.

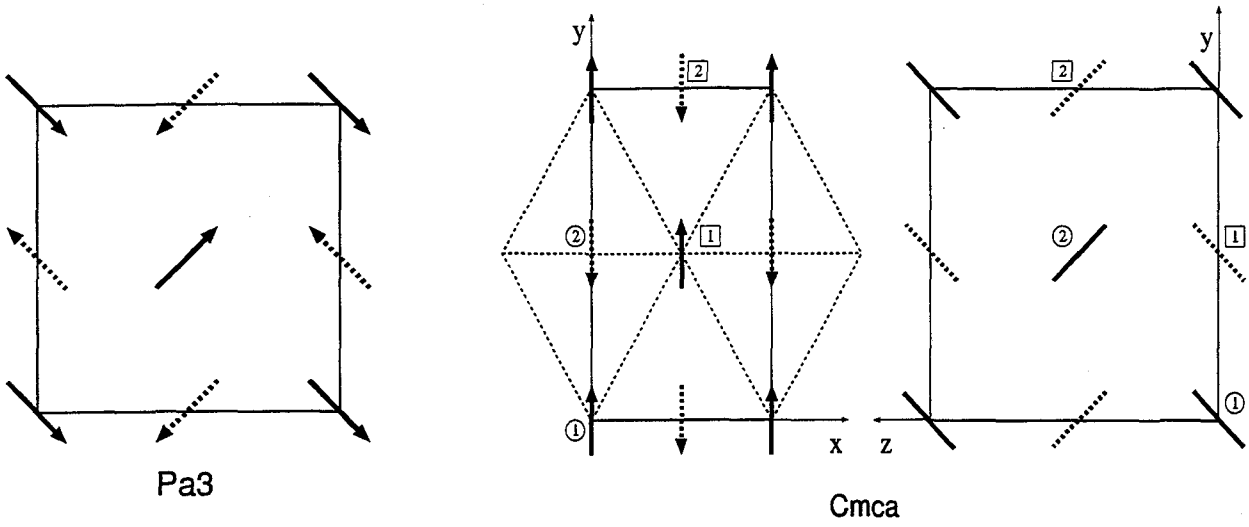

FIG. 11. Comparison of the $Pa3$ with the $Cmca$ structure. For the $Cmca$ the two type of projections are shown: on the x-y and y-z plane. Solid lines represent molecules lying in a c-plane and broken ones in the next c-plane. Arrows indicate the direction of molecular axes whose direction cosines with the z-axes are positive. In the $Pa3$ structure each molecule is along the three-fold axis.

We studied also the band structure in the $Cmc2_1$ changing the displacements of one of the molecular centers of the hcp lattice towards the site of the $Cmca$ structure. The band structures are shown in Fig.14 with m-hcp structure which was first considered to be the structure having metallic bands. In the $Cmc2_1$ structure, the band gap decreases as the displacement of the molecular center increases and the band gap closes at some value of the displacement. In the $Cmca$ structure, the band gap is closed at much lower pressures, lower than about 70 GPa, and the gap is direct.

Those studies presented above for the $Cmc2_1$ and the $Cmca$ structure at pressures above 200 GPa are for fixed orientation of the molecules. In the $Cmc2_1$ structure, however, the molecular orientations are related with the displacement of the molecular centers, so further optimization of the structure are needed.

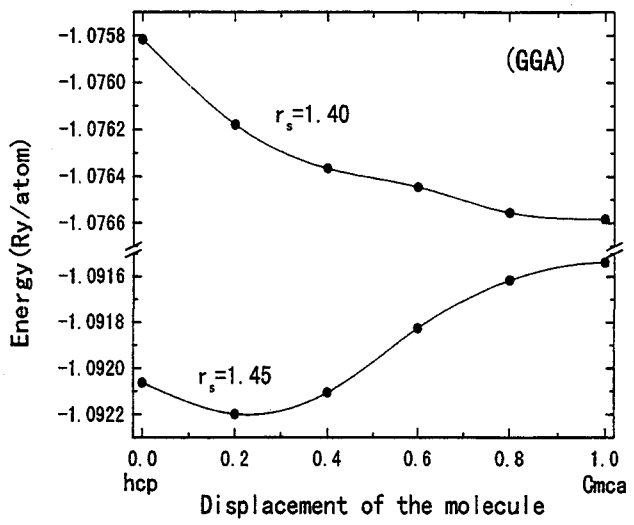

FIG. 12. Total energy in the GGA as a function of the displacement of the molecular center from the hcp site to the *Cmca* site.

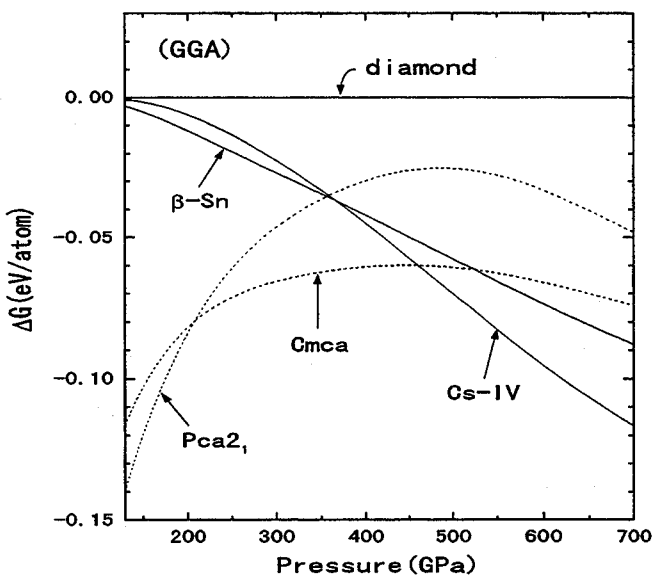

FIG. 13. Gibbs free-energy differences, $\Delta G = G - G_{diamond}$ per atom, calculated from the total energies in the GGA. The solid lines represent the curves for the atomic phase and the broken lines for the molecular phase. The diamond structure is taken to be the reference.

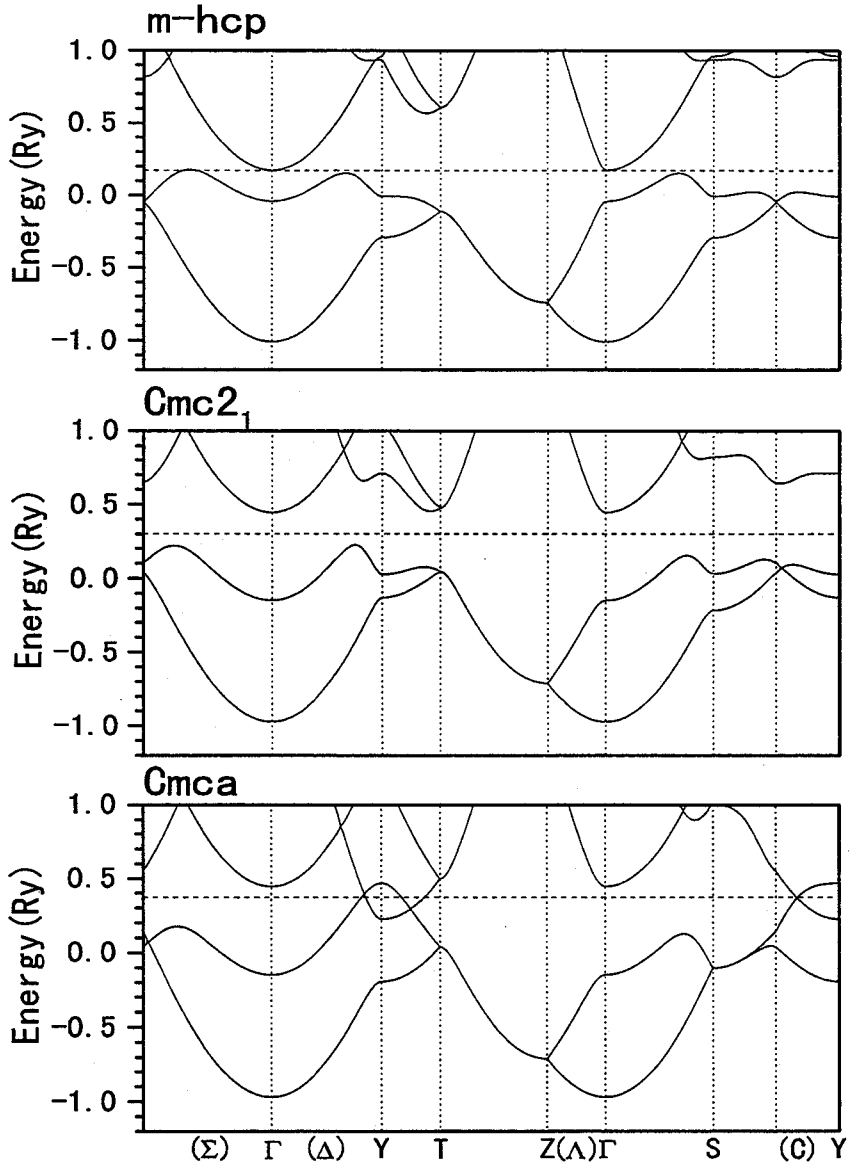

FIG. 14. Changes of the band structures in the GGA among the $Cmc2_1$, the $Cmca$, and the m-hcp structure at $r_s = 1.6$. The base centered orthorhombic unit cell containing two molecules is used for all structures in plotting the band structures with the same axes as that shown for the $Cmc2_1$ in Fig.10. The bond length is set at 1.40 a_0 for all structures and molecular orientation is set at $\theta = 60°$ for the $Cmc2_1$ and the $Cmca$ structure. The m-hcp structure is obtained from the $Cmc2_1$ by setting the molecular orientation along c-axis and the $Cmca$ by displacing the molecular center in the $Cmc2_1$ (See the text). The LDA results are similar to those shown here but the density corresponding to the same band gap is lower than that of the GGA.

III. THE INFRARED AND RAMAN ACTIVE VIBRATIONAL MODES IN THE MOLECULAR PHASE

Very recent Raman and infrared (IR) experiments for the vibrons (intramolecular stretching modes), mid-lying phonons [16] (translational modes of the molecular centers), and other low-lying phonon and librational modes (the motions of the molecular orientation) [21,24] at megabar pressures provide important information on the lattices of the molecular centers and the molecular orientations in the molecular phase of compressed hydrogen. Extensive theoretical studies on the vibrational modes and their frequencies are needed to analyze the experimental data [24] and to determine the structure and orientations of the molecules at megabar pressures.

Many theoretical studies so far, however, have focused mainly on energetics by the use of band theoretical approach [26,29–31] and the studies of the vibrational modes are rather scarce except for the vibrons in the molecular phase. Some studies treated the vibron frequencies based on the *ab initio* calculations [33,41,52], and others treated those based on the effective force constants or the effective pair interactions corrected by *ab initio* calculations [20,53].

Following Cui, Chen, and Silvera's [20] group theoretical analysis, Nagao and Nagara have made *ab initio* calculation of the vibrational frequencies in the molecular phase [50], where they studied the structure with the hcp lattice of the molecular centers and compared with IR and Raman experiments on the vibrons and phonons at megabar pressures.

Very recently the possibility of the fcc lattice of the molecular centers are pointed out experimentally. Also, as studied in the preceding section, possible lattices other than the hcp are proposed theoretically. We study these structures in the following subsections.

A. Group theoretical analysis of vibrational modes at the Γ-point

Goncharov *et al.* pointed out the possibility of the fcc lattice of the molecular centers in the phase II from the selection rules for a Raman phonon line [24]. They observed that the intensity of the peak becomes very weak when the pressure is increased and entered into the region of phase II, and they think that the result shows the line is symmetry forbidden and the molecules sit on the sites with inversion symmetry. They proposed the $Pa3$ or the $Cmca$ structure as are most probable. In the $Pa3$, the molecular centers are on the fcc sites and in the $Cmca$ the molecular centers sit on the face centered orthorhombic lattice sites.

In addition to the experimental study, Kohanoff *et al.* also pointed out that the $Pa3$ structure is located at the local minimum on the energy surface with the energy higher than those of some structures of the hcp lattice from their molecular dynamics study.

In this subsection, we study the vibrational frequencies in the $Pa3$ and the $Cmca$ structures, which are shown again in Fig.11. For the hcp lattice of the molecular centers, the vibrational modes at the Γ-point and their frequencies are calculated by Nagao and Nagara [50]. We follow similar methods of the calculations for the $Pa3$ and the $Cmca$ structure.

We analyze the displacements using the group theory and obtain the symmetry coordinates corresponding to the irreducible representations for the space group [54]. By the use of the symmetry coordinates, we can transform, in advance, the entire force matrix into the reduced form which consists of submatrices on the diagonal. The matrix elements of the submatrices are obtained through the force calculations by the use of the displacements corresponding to the symmetry coordinates which belong to the same irreducible representation. By this treatment, we can calculate the frequencies of the modes belonging to an irreducible representation independently from other modes which belong to other irreducible representations. This treatments can reduce the computational efforts to obtain frequencies corresponding to the modes of interest. They can also enhance the accuracy in the calculation of the matrix elements.

In the construction of the symmetry coordinates, which are constructed from the sym-

metry vectors obtained by the use of projection operators [54], we used ambiguity of the definition of the symmetry coordinates and obtained those which correspond to the vibronic motion, the librational motion, the phonon-like motion, and the uniform translation, so that we can specify the characteristics of the modes. The symmetry coordinates we used are summarized in Table I with those of some other structures.

TABLE I. Characteristics of the symmetry coordinates used in our calculations of the vibrational frequencies at the Γ-point in the Brillouin zone for the $Pca2_1$, the $Cmc2_1$, the $Cmca$, the m-hcp, and the $Pa3$ structures. Each symmetry coordinate is designated by the name of the irreducible representation followed by its characteristics in the parentheses. The letters v, p, l, and t are the characteristics and denote the vibronic, phonon, and librational motions, and the uniform translation, respectively. The θ or ϕ in the parentheses denotes the angle which changes its value by the motion, and x, y, or z the direction of the motion, and xz, or yz the plane in which molecules moves. The vibronic motions in the first row are of in-phase and other vibronic motions are of out-of-phase. The letters, R and I, in the brackets indicate the Raman and IR activities, respectively. Each symmetry coordinate in the same row transfers to that of other structure when one structure is transformed into the other by changing the orientation of the molecules or by displacing the molecular centers, except for those of the $Pa3$.

$Pca2_1$	$Cmc2_1$	$Cmca$	m-hcp[a]	$Pa3$[b]
$A_1(v)$ [R,I]	$A_1(v)$ [R,I]	$A_g(v)$ [R]	$A_{1g}(v)$ [R]	$A_g(v)$ [R]
$A_1(l-\theta)$ [R,I]	$A_1(l-\theta)$ [R,I]	$A_g(l-\theta)$ [R]	$E_{1g}(l-yz)$ [R]	
$A_1(l-\phi)$ [R,I]	—	—	—	$E_g(l)$ [R]
$A_1(p-x)$ [R,I]	—	—	—	$E_g(l)$ [R]
$A_1(p-y)$ [R,I]	$A_1(p-y)$ [R,I]	$B_{1u}(p-y)$ [I]	$E_{2g}(p-y)$ [R]	
$A_1(t-z)$	$A_1(t-z)$	$B_{1u}(t-z)$	$A_{2u}(t-z)$	$T_g(v)$ [R]
				$T_g(v)$ [R]
$A_2(v)$ [R]	—	—	—	$T_g(v)$ [R]
$A_2(l-\theta)$ [R]	—	—	—	
$A_2(l-\phi)$ [R]	$A_2(l-\phi)$ [R]	$B_{1g}(l-\phi)$ [R]	$E_{1g}(l-xz)$ [R]	$T_g^{(1)}(l)$ [R] $T_g^{(2)}(l)$ [R]
$A_2(p-x)$ [R]	$A_2(p-x)$ [R]	$A_u(p-x)$	$E_{2g}(p-x)$ [R]	$T_g^{(1)}(l)$ [R] $T_g^{(2)}(l)$ [R]
$A_2(p-y)$ [R]	—	—	—	$T_g^{(1)}(l)$ [R] $T_g^{(2)}(l)$ [R]
$A_2(p-z)$ [R]	—	—	—	
				$A_u(p)$
$B_1(v)$ [R,I]	—	—	—	

$B_1(l-\theta)$	[R,I]	—		—		—		$E_u(p)$	
$B_1(l-\phi)$	[R,I]	$B_1(l-\phi)$	[R,I]	$B_{2g}(l-\phi)$	[R]	$E_{2u}(l-xz)$		$E_u(p)$	
$B_1(p-y)$	[R,I]	—		—		—			
$B_1(p-z)$	[R,I]	—		—		—		$T_u(t-x)$	
$B_1(t-x)$		$B_1(t-x)$		$B_{3u}(t-x)$		$E_{1u}(t-x)$		$T_u(t-y)$	
								$T_u(t-z)$	
$B_2(v)$	[R,I]	$B_2(v)$	[R,I]	$B_{3g}(v)$	[R]	$B_{1u}(v)$			
$B_2(l-\theta)$	[R,I]	$B_2(l-\theta)$	[R,I]	$B_{3g}(l-\theta)$	[R]	$E_{2u}(l-yz)$		$T_u^{(1)}(p-x)$	[I] $T_u^{(2)}(p-x)$ [I]
$B_2(l-\phi)$	[R,I]	—		—		—		$T_u^{(1)}(p-y)$	[I] $T_u^{(2)}(p-y)$ [I]
$B_2(p-x)$	[R,I]	—		—		—		$T_u^{(1)}(p-z)$	[I] $T_u^{(2)}(p-z)$ [I]
$B_2(p-z)$	[R,I]	$B_2(p-z)$	[R,I]	$B_{2u}(p-z)$	[I]	$B_{2g}(p-z)$			
$B_2(t-y)$		$B_2(t-y)$		$B_{2u}(t-y)$		$E_{1u}(t-y)$			

[a]For the m-hcp, doubly degenerate modes designated by E_{1g}, E_{2g}, E_{1u}, and E_{2u} have two independent symmetry coordinates, respectively.

[b]For the $Pa3$, two triply degenerate librational modes belonging to the T_g representation are distinguished by the superscript $^{(1)}$ and $^{(2)}$, which is the same for the phonon modes belonging to the T_u representation.

B. Computation of force by the frozen phonon and the Hellman Feynman theorem

In the calculation of electronic states, we use the conjugate gradient (CG) minimization technique, in an attempt to use it for the lattice containing more atoms than eight. The CG method can reduce the CPU time and the memory needed for the calculation of electronic states when the matrix is large.

We set the energy cutoff, E_{cut}, of the PW basis at ~65 Ry in our band theoretical calculations at density, $r_s = 1.5$ (P $\sim$ 120 GPa), for which the number of the PW is around 125 $\times N$ (N is the number of atoms in a unit cell). Here the density parameter, r_s, is the radius of the sphere whose volume is equal to the volume per electron in units of Bohr radius, a_0. These values of the energy cutoff are proved sufficient by checking the results with increased energy cutoff of 80 Ry at $r_s = 1.6$.

The condition for the convergence of the electronic wave functions should be set more strict in the calculation of the forces than that needed in the total energy calculations, because the errors in the total energy are of second order in the errors of the wave functions, as is guaranteed by the variational principle for the total energy, while those in the forces are of first order.

The many point sampling in the Brillouin zone is crucial in the total energy calculation of the compressed hydrogen, which is the same in the calculation of the force matrices. Kohanoff *et al.* used $\vec{k} \cdot \vec{p}$ method [41] to obtain the wave functions at points other than the Γ-point from the wave function at the Γ-point. We do not use this method in the present study because the wave functions obtained by this method contains considerable errors at points far from the Γ-point. We sampled about $2000/N$ $\vec{k}$-points in the Brillouin zone, which is proved sufficient in the present studies. We checked the forces by comparing the Hellman-Feynman forces with the derivatives of the total energies with respect to the displacements.

To obtain the force matrix we write the symmetry coordinate as, $q^{ia} = \sum_{n\alpha} C_{ia,n\alpha} r_{n\alpha}$, where i labels the representation and a distinguishes the independent symmetry coordinates

belonging to the same irreducible representation and $r_{n\alpha}$ denotes the Cartesian component, α, of the displacement vector of the atom, n, in the unit cell. And then we calculate the force, $f_{n\alpha}^{ia}$, which mean the Cartesian component, α, of the force acting on the atom, n, when the displacement corresponding to the symmetry coordinate, q^{ia}, is generated in the system. From above quantities we can obtain the force submatrix,

$$\begin{aligned}\Phi_{aa'}^{i} \equiv \frac{\partial^2 E}{\partial q^{ia} \partial q^{ia'}} &= \sum_{n\alpha} C_{ia,n\alpha} \frac{\partial^2 E}{\partial r_{n\alpha} \partial q^{ia'}} \\ &\cong -\sum_{n\alpha} C_{ia,n\alpha} (\triangle f_{n\alpha}^{ia'} / \triangle q^{ia'}),\end{aligned} \tag{1}$$

where E is the total energy per unit cell. And we note that

$$\sum_{n\alpha} C_{ia,n\alpha} C_{i'a',n\alpha} = \delta_{ia,i'a'}, \tag{2}$$

and

$$\sum_{ia} C_{ia,n\alpha} C_{ia,n'\alpha'} = \delta_{n\alpha,n'\alpha'}, \tag{3}$$

as can be shown, for example, from the definition of the symmetry coordinates in Table I of Ref. [50]. The normal coordinates and the frequencies of the vibrational modes are obtained through the diagonalization of the submatrices whose dimensions are much smaller than that of the total force matrix. The matrix elements corresponding to the uniform translations are trivial and the dimensions of the submatrices containing the uniform translation can be reduced further.

C. Pressure dependences of the frequencies and comparison with experiments.

The frequencies calculated in the LDA are shown in Fig.15 for some modes for the $Pa3$ and the $Cmca$ structures. Let us first compare the present results with those obtained for the hcp lattice (Fig.16), we observe that the calculated frequencies of the out-of-phase vibronic modes are higher than that of the in-phase mode, in the fcc lattice also, which is in agreement with the experiments. The frequencies of the mid-lying phonon modes in the

structures with fcc molecular centers are in good agreement with the experiments, which is similar to the results for the structures with hcp molecular centers.

For the $Pa3$ structure, the pressure dependencies of the frequencies are in good agreement with those reported by the experiments for the vibrons and mid-lying phonon modes in phase II. When we compare the results in phase III, the pressure dependences of the vibron frequencies show some discrepancies, but the frequency of the T_u mode, which is the phonon-like modes, is very close to the experiment. The IR activity of this mid-lying phonon T_u mode in the $Pa3$ agrees with the experiment, where an IR phonon mode are observed [16].

However, the rapidly increased and strong IR activity of the vibrons observed in the experiments in phase III shows that this mode is symmetry allowed, which rules out the $Pa3$ structure in the phase III. The $Pa3$ structure has no IR active vibrons, according to the group theoretical analysis. We note here that three vibron IR peaks are reported in phase II [19] although it is not clear that those peaks are symmetry allowed or similar to those observed in the α-N_2 [23].

For the $Cmca$, the calculated frequencies do not agree with the experiments in any phase at pressures lower than 200 GPa as are shown in Fig.15.

Lastly, we mention the low-lying librational modes. The behavior of the pressure dependences of the calculated frequencies for low-lying librational modes is somewhat different from those of the experiments [21,24](Fig.17). Our results for the librational modes are seen in Fig.16 for the $Cmc2_1$. Our frequencies for those modes decrease much slowly as the pressure is decreased, while the experimental values of the frequencies decrease rapidly from the values in phase III and almost vanish at $\sim$ 70 GPa if the curves are extrapolated into phase II. This behavior might be thought to be related with the large orientational fluctuation of the molecules, which can not be treated in the present method. The quantum fluctuation of the molecular orientation will be important even after the orientational order occurred.

We conclude that the frequencies of the vibron and mid-lying phonon modes of the $Pa3$ structure are compatible with the experiments in phase II, but it is ruled out in phase III because of the strong IR activity in phase III. The calculated vibron frequencies of the $Cmca$

do not agree with the experiments at pressures lower than 200 GPa as are shown in Fig.15. However, we note that, if the experimental frequencies are extrapolated to above 250 GPa, the frequencies approach the values calculated in the present study, which supports the possibility of the *Cmca* structure above 250 GPa.

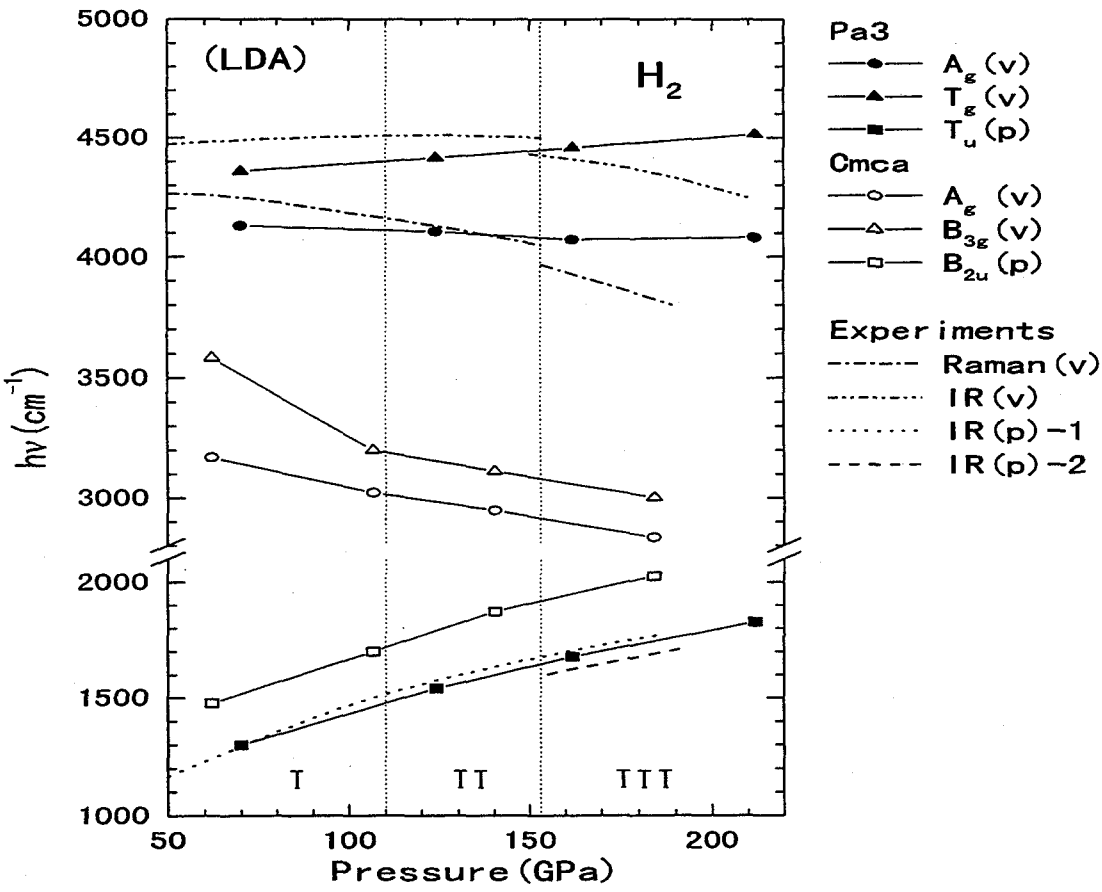

FIG. 15. The pressure dependences of the vibrons and mid-lying phonons in the *Pa*3 and *Cmca* structures. The marks show our data points and lines connecting those points are guides to the eye. The (v), (l), and (p) denote the vibronic, librational, and phonon modes respectively. Experimental data are taken from Ref. [16] (p-H_2) for IR(p)-2 and from Ref. [11] and [55] (o-p mixed H_2) for the others. The vertical dotted lines show the boundaries of the phases I, II, and III taken from Ref. [11] and [47].

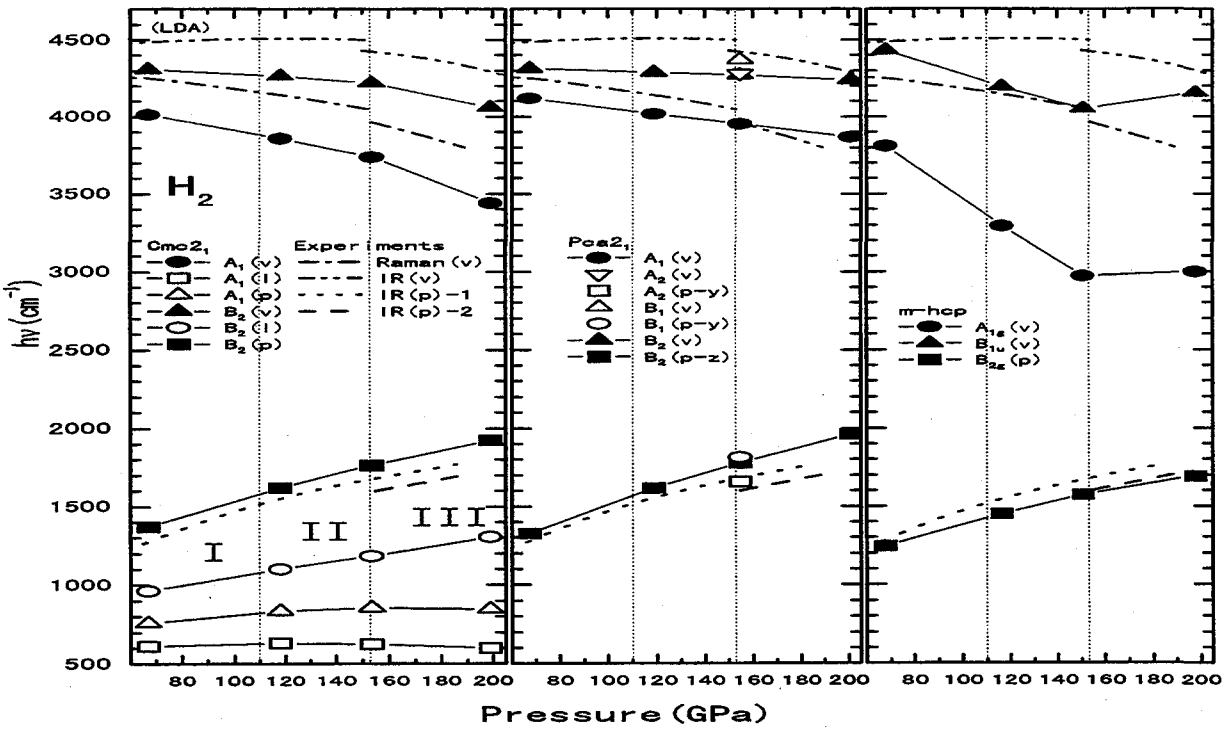

FIG. 16. Pressure dependences of the vibrons and mid-lying phonons in the structures of hcp lattice of molecular centers. The meaning of the symbols and letters designating the lines are same as those explained in Fig.15. (From Ref. [50])

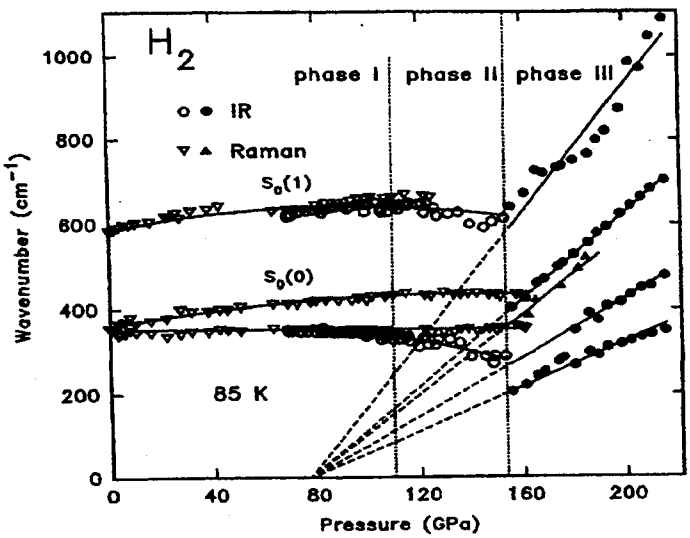

FIG. 17. Pressure dependences of the low-lying Raman peaks for Hydrogen. (From Ref. [21])

IV. DISPERSIONS OF THE VIBRATIONAL FREQUENCIES AND THE ZERO-POINT ENERGY OF THE PROTON MOTIONS

Total energies studied above do not include the zero-point energy (ZPE) of the proton motions. The effects of the proton motions have long been thought to be important in hydrogen, which is the lightest of natural elements. Straus and Ashcroft [32] pointed out that the static energy of an anisotropic structure which is lower than those of the cubic structures becomes higher when the ZPE is taken into account. Their study used the self-consist phonon approach based on the second order perturbational theory treating the atomic potential as the perturbation to the uniform electron gas, which is of lowest order and further studies are needed.

Recently Natoli *et al.* [34] studied the diamond structure and the simple hexagonal structure which is one of the anisotropic structures of filament-like, using the diffusion Monte Carlo method which is one of the quantum Monte Carlo (QMC) approaches treating both electronic and protonic motions quantum mechanically. They proposed that the energy of the diamond structure becomes lower than the simple hexagonal structure at low densities in the atomic phase when the ZPE is taken into account. In the following paper, they also studied the structures in the molecular phase and reported that the ZPE's are nearly same when the lattice of the molecular centers are same [35].

The QMC, which was first applied to the hydrogen by Ceperley *et al.* [56], is exact, in principle, except for the negative sign problem of the wave function for Fermion system. In addition to the sign problem, the computer resources available at present, limit the accuracy of the results with considerable numerical errors. And further studies may be needed to confirm the results.

In this section, we attempt to calculate the ZPE for some structures in both the atomic and the molecular phases, in the harmonic approximation.

A. Obtaining the dispersions in the LDA band calculation

To calculate the ZPE, we need the vibrational frequencies for all modes at all points in the Brillouin zone, which require, in principle, the forces of all ranges of the interaction. The linear response theory [57](for a review, see Ref. [58]) enables us to calculate those forces by the use of perturbational approach. The computations, however, are complicated when the electrons are in the Bloch states. On the other hand, direct methods in which the forces are calculated either from the electron density obtained by the band calculation through Hellman-Feynman theorem or from the change of the energy due to the atomic displacements, are less complicated and straightforward.

We adopt the direct method using the Hellman-Feynman theorem and the supercell containing up to 32 atoms. Using the force constants among atoms in the supercell, we can construct the dynamical matrix as is studied in the following subsection. The band calculations are done using the CG method developed in the studies of the last section by which structures containing large number of atoms in the unit cell can be treated. As the number of the atoms in the unit cell is increased keeping the energy cut-off of the PW fixed, the number of the PW needed to expand the electronic states increases, by which the dimension of the Hamiltonian matrix becomes very large. The CG minimization technique requires less CPU time in the calculation of the eigen states than the usual diagonalization technique when the dimension of the matrix is large [59]. The supercell method which we will employ in the calculation of the force constants requires a lot of PW basis functions, but less numbers of $\vec{k}$-points and the CG method is suitable for the present band calculation. Typically, in our calculations about 4000 PW basis functions and $3 \times 3 \times 3$ $\vec{k}$-point mesh are used for the supercell containing 32 atoms which consists of 8 to 16 primitive cells. With this number of the plane waves, we can set the energy cutoff of $\sim$75[Ry] at $r_s = 1.35$ and $\sim$95[Ry] at $r_s = 1.2$.

To avoid the anomalous behavior of the forces due to the discontinuous change of the occupancy of the electronic states at the Fermi-surface, we used the Gaussian smearing

method [60]. This method helps to reduce the numbers of $\vec{k}$-points and to reduce the CPU time.

We did not apply GGA to the exchange-correlation energy to save the computation time in the calculations of the force matrices. This causes about 10 % smaller values of the vibron frequency but the difference is much smaller for other modes [61]. The error can be thought smaller in the atomic phase where the electron densities are less localized than the molecular phase, because the GGA favors the localization of the electron density.

B. Calculation of the force constants and the interpolation of the frequencies over the Brillouin zone

We use the method which Parlinski *et al.* studied the phonon dispersion and reported its efficiency in their recent paper [62]. We define the supercell containing several primitive cells. When one of the atoms, say ν-th atom in the 0-th primitive cell, in the supercell is displaced with the displacement $\vec{u}(0,\nu)$, the force, $\vec{F}(\mathrm{n},\mu)$, acting on the μ-th atom in the n-th primitive cell, is written in the harmonic approximation,

$$\vec{F}(n,\mu) = -\sum_{L} \mathbf{B}(n,\mu;L,\nu)\cdot\vec{u}(0,\nu) \tag{4.1}$$

$$= -\mathbf{B}_L(n,\mu;0,\nu)\cdot\vec{u}(0,\nu), \tag{4.2}$$

where $\mathbf{B}(n,\mu;L,\nu)$ denotes the harmonic force constant matrix between the atoms (n,μ) and (L,ν) which is (3×3), and $\mathbf{B}_L(0,\mu;L,\nu)$ is the force constant in the supercell approximation. In the above equation, the summation over the label L comes from the supercell method in which the equivalent atoms in every supercell displace in the same manner.

Using above force matrices, dynamical matrix $\mathbf{D}(\vec{k})$ for the crystal is written

$$\mathbf{D}(\vec{k};\mu,\nu) = \frac{1}{\sqrt{M_\mu M_\nu}}\sum_{m}\mathbf{B}(0,\mu;m,\nu)\ \exp[-2\pi i\vec{k}\cdot\{\vec{R}(0,\mu)-\vec{R}(m,\nu)\}] \tag{4.3}$$

where M_μ and $\vec{R}(m,\mu)$ denote the mass of the atom and its original position respectively and the summation m runs over all atoms in the crystal.

Next, we replace the $\mathbf{B}(0,\mu;m,\nu)$ by the $\mathbf{B}_L(n,\mu;L,\nu)$ of the supercell approximation and define the dynamical matrix $\mathbf{D}_L(\vec{k})$ in the supercell approximation,

$$\mathbf{D}_L(\vec{k};\mu,\nu) = \frac{1}{\sqrt{M_\mu M_\nu}} \sum_\kappa w_\kappa \mathbf{B}_L(0,\mu;\kappa,\nu) \ \exp[-2\pi i \vec{k} \cdot \{\vec{R}(0,\mu) - \vec{R}(\kappa,\nu)\}] \tag{4.4}$$

In the above equation, the summation over κ runs over the atoms in a supercell and should be taken isotropically from the atom $(0,\mu)$ we are considering, which leads to the matrix, $\mathbf{D}_L$, of hermitian. To remove the overcounting of the contribution from the atoms on the supercell boundary, the wait w_κ is introduced.

The dynamical matrices $\mathbf{D}_L(\vec{k})$ and $\mathbf{D}(\vec{k})$ coincide at several points in the Brillouin zone, $\vec{k}_L$, satisfying the condition,

$$\exp(2\pi i \vec{k}_L \cdot \vec{L}) = 1. \tag{4.5}$$

This condition means that the $\vec{k}_L$ is the reciprocal lattice points for the super-lattice $\vec{L}$. The dynamical matrices at points other than the $\vec{k}_L$'s are thought to be those obtained by some kind of interpolation. The interpolation will become more accurate when the supercell grows larger, because the number of the accurate points $\vec{k}_L$ in the Brillouin zone increases as the supercell grows larger.

C. Dispersion curves and the stabilities of the structures

We perform the calculations for some structures of interest in the atomic phase as well as in the molecular phase. In the atomic phase, we take the tetragonal diamond family with special attention to the $Cs-IV$ and the $\beta-Sn$ structure. Those are important structures because they have been pointed out as the structures having low energy near the pressure of molecular dissociation, which are studied in section II. In the molecular phase, we take the $Cmca$ structure. Those structures are shown in Figs.7 and 11.

For the $Cs-IV$ and $\beta-Sn$ structures we calculated the force constant matrices among 32 atoms using the supercell consisting of 16 primitive cells each of which contains two

atoms. For the $Cmca$ structure, we similarly calculated the force matrices among 32 atoms in the supercell which consists of 8 primitive cells each of which contains 4 atoms.

Owing to the symmetry of the structure, some force constant matrices are obtained from other force constant matrix by the symmetry operations. Those symmetry consideration also restricts the shapes of the force constant matrices. Although the present treatment do not necessarily need the symmetry operations, we used them to restrict the elements of the force matrix and to check the results.

The total dynamical matrices of the system at each $\vec{k}$-points are obtained by the use of those force constant matrices, which are 6×6 for the $Cs-IV$ and the $\beta - Sn$ and 12×12 for the $Cmca$ structure.

The frequencies thus obtained are shown in Fig.18(a) for the $Cs-IV$ structure at $r_s = 1.3$ ($P \sim 300GPa$). The points of exact frequencies are shown by solid squares in the figures. The "interpolation" frequencies shown by the doted lines between the exact points may have some errors, because the number of the mesh points of the exact value is small. The frequencies at all points of exact values are real, which means that this structure is stable as a whole. [63] As the density is increased, the frequencies increase due to the increase of the interaction among the atoms which is shown in Fig.18(b) at $r_s = 1.1$ ($P \sim 1200GPa$).

In Fig.19, we show the results for the $\beta - Sn$ structure. In the $\beta - Sn$ structure, there are 6 modes of which 2 mode are unstable. The large values of the imaginary frequencies mean strong instabilities in this structure. In the cubic diamond structure, 3 optical phonon modes become unstable. The instability in the cubic diamond has been pointed out from the total energy calculations [31], as is shown in section II. The frequencies in this structure also show strong instabilities.

For the $Cmca$ structure in the molecular phase, we show the results in Fig.20 at $r_s = 1.35$. This structure has 12 modes at each $\vec{k}$-point and some of them is unstable as can be seen in the figure.

Here we study the instabilities of the $Cmca$ structure in relation to the imaginary frequency mode at the Γ-point. This mode corresponds to the displacements of the atoms

towards the $Cmc2_1$ structure. As we studied the structures above 200 GPa in section II, the $Cmca$ is the limiting structure of the $Cmc2_1$ corresponding to the special value of the displacement of the molecular center and possible optimization change the stable region for the $Cmca$. To study the stable region of the $Cmc2_1$ structure, we performed some more optimization of the $Cmc2_1$ structure by changing the molecular orientations. The results of the similar calculation carried out in the section II are shown in Fig.21. With this optimization, the $Cmca$ is located at the local maximum of the energy. The height of this energy hump, however, is very low which is lower than 0.2 mRy and the displacement from the $Cmca$ is also small. This hump remains to higher pressures, as are shown in the same figure.

Those results show that the $Cmc2_1$ structure is stable above 200 GPa and that the structures at even higher pressures are probably very close to the $Cmca$ structure. This is in accordance with the Kohanoff [41]'s MD observation that the averaged structure becomes $Cmca$ at elevated temperature above 70 K.

Another unstable mode at the Y-point in the Brillouin zone correspond to the displacement of the molecular center in the $Cmca$ structure with doubled unit cell along y-direction. The imaginary frequency of this mode is less than 400 cm^{-1} and we will need more accurate calculations. We would like to point out also that, if more sophisticated calculation such as the self-consistent phonon approach is used in the calculation, some unstable modes may become stable due to the renormalization effect on the frequency. The renormalized frequencies, however, may still remain low if they become stable.

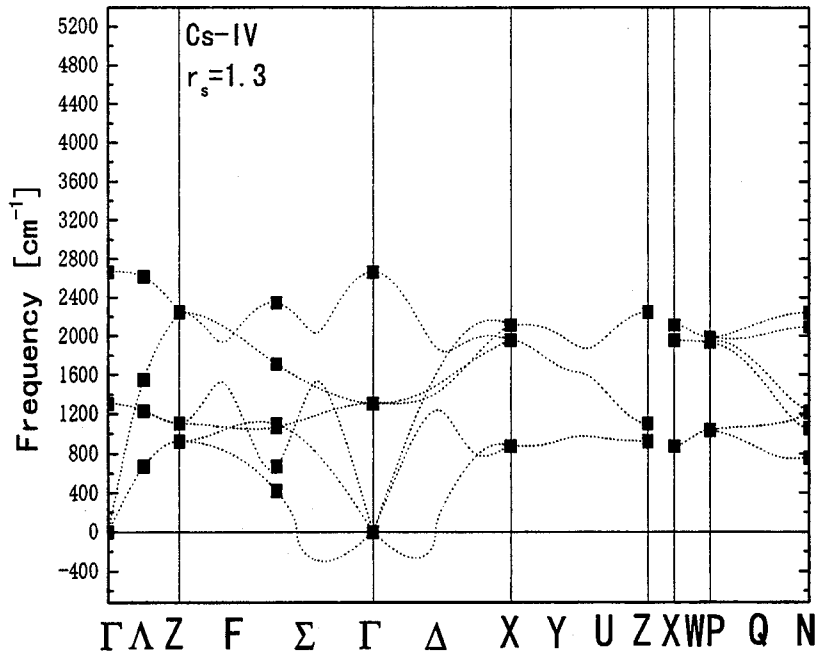

(a) $Cs-IV$ structure , r_s=1.3($P \sim 300GPa$)

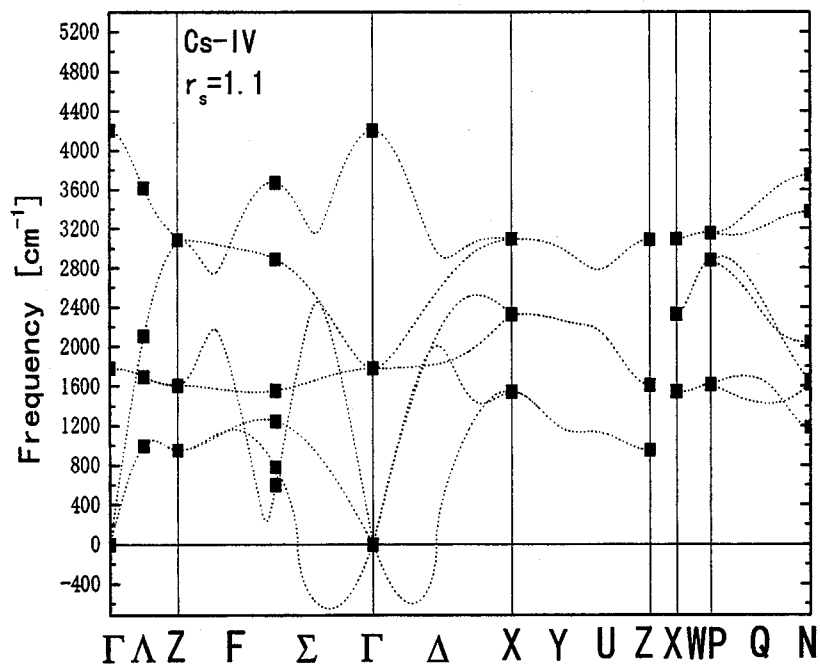

(b) $Cs-IV$ structure , r_s=1.1($P \sim 1200GPa$)

FIG. 18. Phonon dispersions of compressed hydrogen in the $Cs-IV$ structure. The solid squares and doted lines indicate exact calculation points and interpolation curves respectively.

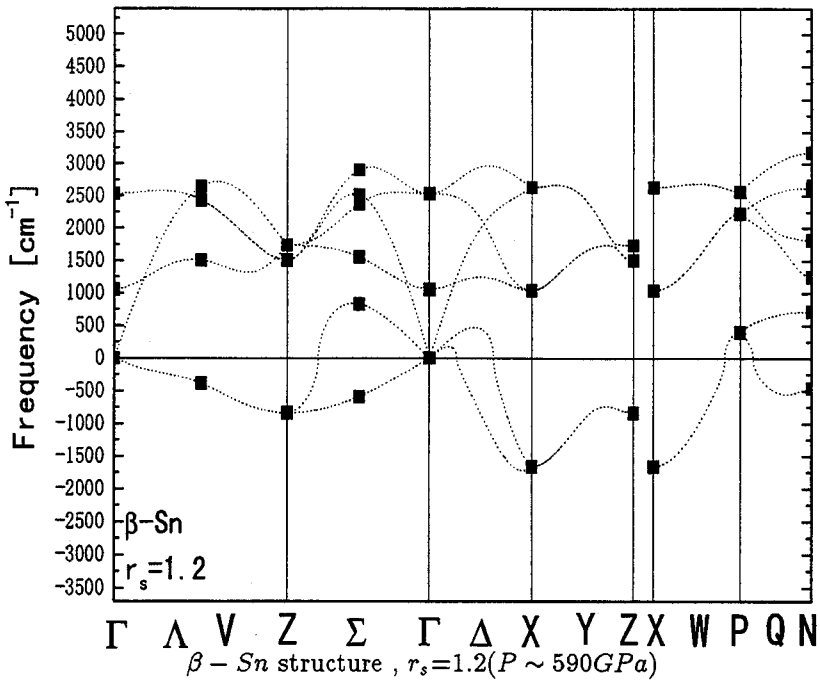

FIG. 19. Phonon dispersions of compressed hydrogen in the $\beta - Sn$ structure. The solid squares and doted lines indicate exact calculation points and interpolation curves respectively.

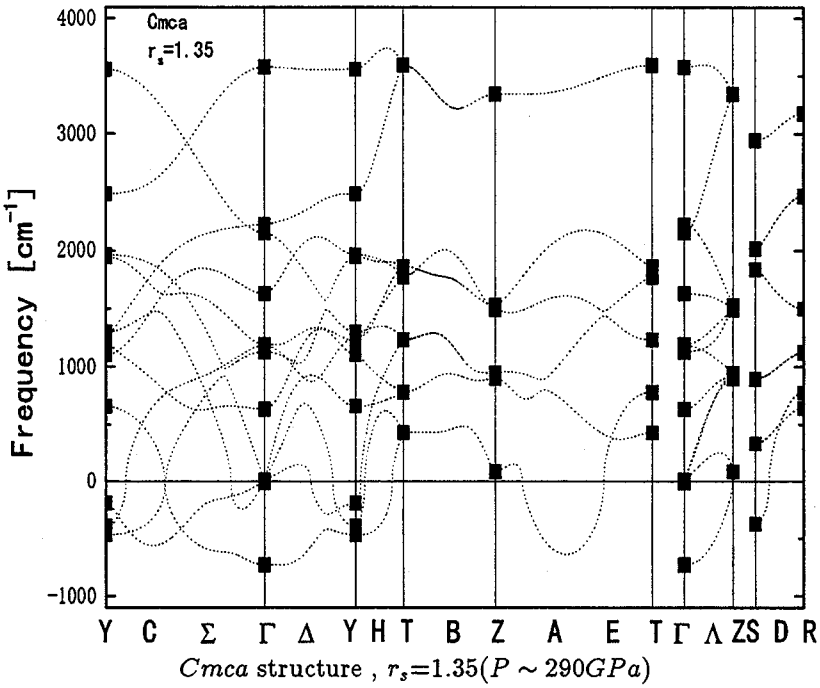

FIG. 20. Phonon dispersions of compressed hydrogen in the *Cmca* structure. The solid squares and doted lines indicate exact calculation points and interpolation curves respectively.

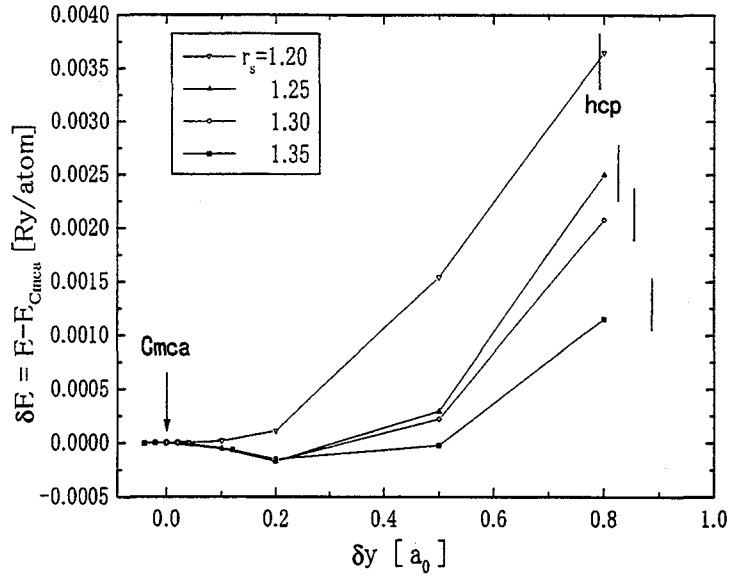

FIG. 21. Total energy difference as functions of the displacement of the molecular center from the *Cmca* site to the hcp site.

D. Evaluation of the ZPE for some structures

Using above vibrational frequencies at some of the points in the Brillouin zone, we evaluate the ZPE for the structures studied above ,where we sampled 64 k-points in the Brillouin zone.

The $Cs-IV$ has stable modes at almost all region of the Brillouin zone. In other structures, some modes are unstable as are shown in the preceding subsection. However, the unstable modes are rather small portion for the *Cmca* structure. We think we can approximately evaluate the ZPE by discarding the contributions from the frequencies of the unstable modes, because the short range structure, which determine the high frequency modes, do not differ appreciably from the *Cmca* and also because the modes with small imaginary frequencies will remain low frequency modes even if they become stable by other approaches.

We calculate the ZPE for the $Cs-IV$ in the atomic phase and the *Cmca* structure as the representative in the molecular phase. We show also the ZPE for the $\beta-Sn$ though it

has many unstable modes and other approaches may be needed.

In Table II, we summarize the total energy in the clamped nuclei approximation, E_{st}, which we studied in section II, and the ZPE, E_{zp}, for the $Cs-IV$, $\beta-Sn$ in the atomic phase and for the $Cmca$ in the molecular phase with some structural parameters.

We first compare our results in the atomic phase with those of Kagan *et al.* [64] which are obtained by the perturbational approach and accurate at high densities. They observed the general tendency that the ZPE is lower for the structures with high coordination, fcc and hcp, for example, than those with low coordination, planar and filamentary when they are compared at the same density. In Fig.22, we plotted our data with some data by Kagan *et al.*. We note here that the values of the ZPE of present calculation are very close to those obtained by Kagan *et al.*. Straus and Ashcroft [32] showed that the ZPE of sc is lower than that of anisotropic filamentary structure.

TABLE II. The total energy in the clamped nuclei approximation E_{st} and the zero-point energy E_{zp} with some structural data.

		$Cs-IV$			$\beta-Sn$	
$r_s[a_0]$	c/a	E_{st}[Ry]	E_{zp}[Ry]	c/a	E_{st}[Ry]	E_{zp}[Ry]
1.0	2.915	-0.74345	0.03674	0.7384	-0.73799	0.02926
1.1	2.853	-0.88292	0.02911	0.8131	-0.88048	0.02575
1.2	2.786	-0.97236	0.02357	0.8360	-0.97112	0.02062
1.3	2.707	-1.02981	0.01957	0.9099	-1.02998	0.01851

		$Cmca$		
$r_s[a_0]$	$\rho[\AA]$	$\theta[degree]$	E_{st}[Ry]	E_{zp}[Ry]
1.2	0.845	46.1	-0.971172	0.02400
1.25	0.871	39.4	-1.004043	0.02236
1.3	0.873	37.4	-1.030423	0.02097
1.35	0.814	40.2	-1.051963	0.01960

We next compare our results with those of Natoli *et al.* [34,35] who studied the filamentary structure of atomic phase and an assumed structure in the molecular phase by the QMC. They obtained that the ZPE of the atomic phase is lower than that of the molecular phase in agreement of our results. The pressure from the ZPE is in agreement with Natoli *et al.*'s. Our values, however, are nearly a half of those obtained by them. The ZPE of their $Cmc2_1$ is 45 mRy at $r_s = 1.31$ which corresponds to averaged frequency of $\sim 3290\ cm^{-1}$. This value seems to be too large because the averaged values lie nearly maximum value of our vibrational frequencies.

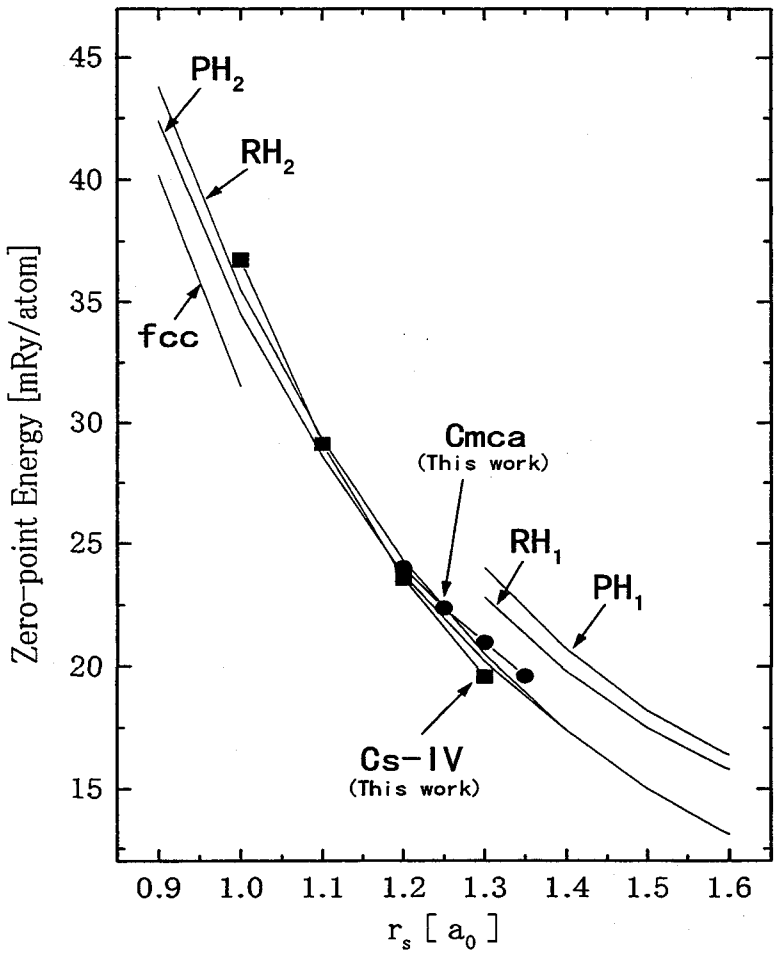

FIG. 22. Zero-point Energy of the $Cs-IV$ and $Cmca$ structure. The marks show our data points and the lines connecting those points are guides to the eye. Zero-point Energy of other structures are from Ref. [64]

E. Effects of the ZPE on the Pressure of Molecular Dissociation

Adding the ZPE to the total energy, we discuss the molecular dissociation assuming the atomic phase to be $Cs-IV$ and the molecular phase the $Cmca$ structure. The condition of the phase transition, when the ZPE is omitted, is given by,

$$E^m_{st}(V_m) + pV_m = E^a_{st}(V_a) + pV_a$$

$$p = -\frac{E^m_{st}(V_m) - E^a_{st}(V_a)}{V_m - V_a} = -\left(\frac{\partial E^m_{st}}{\partial V}\right)_{V=V_m} = -\left(\frac{\partial E^a_{st}}{\partial V}\right)_{V=V_a}$$

These equations are the equal condition of the the Gibbs free energies, which is identical with enthalpy in the present case of $T = 0$, between the atomic and molecular phases. In the above equations, V_m and V_a denote the volume of the molecular phase and that of the atomic phase respectively between which the transition occur. Using the density parameter r_s the volume in units of a_0^3 is written, $V = (4\pi/3)r_s^3$.

The values of the r_s between which the transition occur are 1.246 and 1.253 for the atomic and molecular phase respectively, which means the volume change associated to the transition is less than 2 %.

When the ZPE is taken into account, the transition pressure changes from p to $p + \Delta p$, and the volume changes of both phases are ΔV_m and ΔV_a, for the molecular phase and the atomic one, respectively. Then the condition is given by,

$$E^m_{st}(V_m + \Delta V_m) + E^m_{zp}(V_m + \Delta V_m) + (p + \Delta p)(V_m + \Delta V_m)$$

$$= E^a_{st}(V_a + \Delta V_a) + E^a_{zp}(V_a + \Delta V_a) + (p + \Delta p)(V_a + \Delta V_a) \quad .$$

We observe that the ΔV_m and ΔV_a are about 3 % for both phases, at the transition volumes. Expanding this both sides of above equation to first order terms and using the the conditions for the static case, we obtain,

$$E^m_{zp}(V_m) + \Delta p V_m = E^a_{zp}(V_a) + \Delta p V_a$$

from which we obtain the shift of the transition pressure,

$$\Delta p = -\frac{E^m_{zp}(V_m) - E^a_{zp}(V_a)}{V_m - V_a} \quad .$$

The volume changes are given, to the first order, by

$$\Delta V_m = -\frac{\Delta p - p^m_{zp}}{(\partial^2 E^m_{st}/\partial V^2)} \quad ,$$

and

$$\Delta V_a = -\frac{\Delta p - p^a_{zp}}{(\partial^2 E^a_{st}/\partial V^2)} \quad ,$$

where the right hand side is evaluated at each transition density without ZPE, and p^m_{zp} and p^a_{zp} are the pressure contributions from the ZPE. The shift of the transition pressure of the $Cmca$ to the $Cs - IV$ is -60 GPa. The same quantity for the deuterium is divided by the factor of $\sqrt{2}$, which means the transition pressure of deuterium is higher than those of hydrogen.

At the transition pressure, the contribution from the ZPE to the total pressure is about 30 GPa which is about 10 % of the total pressure.

V. STRUCTURES OF COMPRESSED HYDROGEN AND MOLECULAR DISSOCIATION WITH METALLIC TRANSITION

We studied, in section II the total energy in the clamped nuclei approximation and in section III, the vibrational frequencies for some of recently proposed structures with, in section IV, the vibrational frequencies at some points in the Brillouin zone for some of the possible structures in both atomic and molecular phases. Combining the information obtained by the present study and those obtained before, we discuss the structures and the possible scenario to the molecular dissociation with the metallic transition.

A. From the view point of the static energy

From the total energy calculations in the clamped nuclei approximation we obtained the Gibbs free energies and compared those among some candidate structures.

At pressures lower than around 100 GPa, the energy differences among structures with various orientational patterns are very small when the molecular centers are on the same lattice, which implies that the molecules are in a rotational states or in states with large orientational fluctuations if they are ordered. The structures with the fcc lattice of the molecular centers, of which the lowest energy structure of orientational order is the $Pa3$, are of higher energy than the $Pca2_1$ of the hcp lattice at pressures above $\sim$ 50 GPa.

As the pressure becomes higher than around 150 GPa the energy differences becomes considerably large, which implies that the molecules are orientationally ordered in some pattern of the orientation at those pressures. In the structures with hcp lattice of the molecular centers, the $Pca2_1$ structure or the $Cmc2_1$ is most probable. However, at pressures near 200 GPa, molecular centers begins to move from the hcp sites to those of other lattice which the recent theoretical studies predict to be base centered orthorhombic lattice. The total energy of the $Cmc2_1$ in this region will need study with some more optimization.

Detailed study of the $Cmc2_1$ and the $Cmca$ structures above 200 GPa revealed that the

energy of the $Cmc2_1$ structure becomes slightly lower than the $Cmca$ structure and $Cmc2_1$ structure approaches to the $Cmca$. And the $Cmc2_1$ or the $Cmca$ persist up to $\sim$ 450 GPa.

Around 450 GPa the structures in the atomic phase becomes lower than those in the molecular phase. In this region of the pressure, the $Cs-IV$ structure is of lowest energy. The anisotropic planar structure is predicted in the small region around 1.7 TPa [31]. The isotropic hcp structure will appear around 2 TPa and bcc over 4 TPa [43].

Let us here study the band overlapping in the molecular phase and discuss the metallic transition. The GGA band gaps in the $Pca2_1$ persist over 200 GPa and those of the $Cmc2_1$ close near 200 GPa. The GGA also underestimates the band gaps [61] and the pressures will shift upward by $\sim$ 100 GPa [28]. We note that the band gaps of the structures in which the molecules keep away with each other persists to higher energy. For example, the energy gaps of the $Pa3$ structure persists over 200 GPa, which is similar to the $Pca2_1$ of the hcp lattice. The band gaps of the $Cmca$ close above $\sim$ 60 GPa and already metallic in the region above $\sim$ 300 GPa. The $Cmca$ structure which is very close to the $Cmc2_1$ structure in this region of the pressure can not be ruled out there.

B. From the view point of the vibrational frequencies

The vibrational modes and their frequencies with the dispersions of the vibrational frequencies add some more insight into the structures in both atomic and molecular phases.

Our calculations of the frequencies are performed for the structures in which the molecules are oriented in some patterns and we may not be able to compare the results with the experimental ones in the phases where the molecules are in the rotating state or in the states of large orientational fluctuations which are expected in phase II. However, we think that our treatment can approximately deal with the frequencies of the vibrons and the mid-lying phonons if the frequencies do not depend significantly on molecular orientations. In fact, it is the case when the density becomes lower than $\sim$ 100 GPa, as is observed in the small differences of the calculated vibrons and phonon frequencies among those in different

molecular orientations. So we compared the results with experiments in section III for some modes.

Our results imply that the structure most probable in phase II is the hcp lattice with molecules in partial order or in ordered structure with large orientational fluctuation. The $Pa3$ structure, with large orientational fluctuation, is not ruled out from the view point of the vibron and mid-lying phonon frequencies, because weak peaks in the IR experiments may be expected for the symmetry forbidden vibrons like α-N_2 [65] owing to lattice distortions.

And in phase III, the calculated frequencies of vibrons and mid-lying phonons suggests the $Cmc2_1$ structure most probable. The frequencies of the vibrons and mid-lying phonons in the $Cmca$ contradict the experiments at pressures lower than 200 GPa. We note that, if the experimental frequencies are extrapolated to above 250 GPa, the frequencies approach the values calculated in the present study, which supports the $Cmca$ or $Cmca$-like structures above 250 GPa. There exists no available data of IR and Raman experiments.

VI. CONCLUSIONS AND REMARKS

The vibron and the mid-lying phonon frequencies for the $Pa3$ structure is compatible with the experimental results in phase II, although this structure has the total energy higher than the hcp structures in the pressure range of the phase II, [26,30,31] and has no IR active vibron modes in the pure systems. However, weak IR signal may be observed in the mixed system of the ortho- and para- species or in the system with lattice distortions, where the present analysis of the activities can not be applied. If the $Pa3$ structure is realized in phase II, the mid-lying phonon mode should be observed in the IR experiments [16] for which there is no experimental data.

In the molecular phase above 200 GPa, we studied the $Cmc2_1$ and the $Cmca$ structures. The $Cmc2_1$ structure is very close to the $Cmca$ structure and approaches to the $Cmca$ at higher pressures. The total energy of the $Cmc2_1$ in the clamped nuclei approximation is slightly lower than the $Cmca$ but the energy difference is very small. The $Cmca$ structure is not ruled out at pressures higher than $\sim$ 350 GPa.

We studied the phonon dispersion and the ZPE with its effects on the transition pressures. Our results show that the phonon dispersion in the $Cs-IV$ suggests that the $Cs-IV$ is stable and probable in the atomic phase. In the molecular phase we studied the ZPE for the structure $Cmca$ as the representative. The magnitude of our ZPE is much less than those obtained by Ceperley *et al.* which seems to be too large as is discussed in section IV.

The pressure of the molecular dissociation for hydrogen is $\sim$ 400 GPa according to our study including the effects of the ZPE and that for the deuterium is slightly higher by $\sim$ 30 GPa.

Our present results suggest that the metalization occurs by the band overlapping above $\sim$ 300 GPa, although the estimation of the band gap may need more studies by the calculation beyond the LDA.

At this end of the paper, we refer the results of recent path-integral molecular dynamics approach [66] to the quantum effects on the equilibrium position of the hydrogen atoms in

the silicon lattice [67], in which the results show rather classical behavior of hydrogen in the lattice. This may justify the present approach which starts from the study by the classical treatment of the proton motion and later takes the quantum correction into account.

REFERENCES

[1] E. Wigner and H. B. Huntington, J. Chem. Phys. **3**, 764 (1935).

[2] D. E. Ramaker, L., Kummer, and F. E. Harris, Phys. Rev. Lett. **34**, 812 (1975).

[3] C. Friedli and N. W. Ashcroft, Phys. Rev. B**16**, 662 (1977).

[4] A. A. Abrikosov, Sov. Phys. JETP **12**, 1254 (1961).

[5] N. W. Ashcroft, Phys. Rev. Lett. **21**, 1748 (1968).

[6] T. Schneider and E. Stoll, Physica **55**, 702 (1971).

[7] M. D. Whitmore, J. P. Carbotte, and R. C. Shukla, Can. J. Phys. **57**, 1185 (1979).

[8] T. W. Barbee III and M. L. Cohen, Phys. Rev. B**43**, 5269 (1991).

[9] C. F. Richardson and N. W. Ashcroft, Phys. Rev. Lett. **78**, 118 (1997).

[10] See, for example, *Jupiter* (The University of Arisona Press, Tucson, Arisona 1976), ed. T. Gehrels.

[11] H. K. Mao and R. J. Hemley, Rev. Mod. Phys. **66**, 671 (1994); and references therein.

[12] S. T. Weir, A. C. Mitchell, and W. J. Nellis, Phys. Rev. Lett. **76**, 1860 (1996); and references therein for earlier dynamic compression experiments.

[13] M. Hanfland, R. J. Hemley, and H. K. Mao, Phys. Rev. B**43**, 8767 (1991); J. H. Eggert *et al.*, Phys. Rev. Lett. **66**, 193 (1991); A. L. Ruoff and C. A. Vanderborgh, Phys. Rev. Lett. **66**, 754 (1991); **71**, 4279(E) (1993).

[14] L. B. Da Silva *et al.*, Phys. Rev. Lett. **78**, 483 (1997).

[15] W. J. Nellis, M. Ross, and N. C. Holms, Science **269**, 1249 (1995).

[16] N. H. Chen, E. Sterer, and I. F. Silvera, Phys. Rev. Lett. **76**, 1663 (1996).

[17] R. J. Hemley *et al.*, Phys. Rev. Lett. **76**, 1667 (1996).

[18] P. Loubeyre *et al.*, Nature, **383**, 702 (1996).

[19] L. Cui *et al.*, Phys. Rev. Lett. **72**, 3048 (1994).

[20] L. Cui, N. H. Chen, and I. F. Silvera, Phys. Rev. B**51**, 14987 (1995); B**57**, 656(E) (1998); and references therein.

[21] I. I. Mazin *et al.*, Phys. Rev. Lett. **78**, 1066 (1997).

[22] A. F. Goncharov *et al.*, Phys. Rev. Lett. **75**, 2514 (1995).

[23] A. F. Goncharov *et al.*, Phys. Rev. B**54**, R15590 (1996).

[24] A. F. Goncharov *et al.*, Phys. Rev. Lett. **80**, 101 (1998).

[25] For the hydrogen(deuterium) molecule para designates the even(odd) rotational quantum number, J, and ortho the odd(even) J species.

[26] T. W. Barbee III, A. Garcia, and M. L. Cohen, Phys. Rev. Lett. **62**, 1150 (1989).

[27] N. W. Ashcroft, Phys. Rev. B**41**, 10963 (1990), and references therein.

[28] H. Chacham and S. G. Louie, Phys. Rev. Lett. **66**, 64 (1991).

[29] E. Kaxiras, J. Broughton, and R. J. Hemley, Phys. Rev. Lett. **67**, 1138 (1991).

[30] H. Nagara and T. Nakamura, Phys. Rev. Lett. **68**, 2468 (1992).

[31] K. Nagao, H. Nagara and S. Matsubara, Phys. Rev. B**56**, 2295 (1997).

[32] D. M. Straus and N. W. Ashcroft, Phys. Rev. Lett. **38**, 415 (1977).

[33] M. P. Surh, T. W. Barbee, and C. Mailhiot, Phys. Rev. Lett. **70**, 4090 (1993).

[34] V. Natoli, R. M. Martin, and D. M. Ceperley, Phys. Rev. Lett. **70**, 1952 (1993).

[35] V. Natoli, R. M. Martin, and D. M. Ceperley, Phys. Rev. Lett. **74**, 1601 (1995).

[36] E. G. Brovman, Yu. Kagan, and A. Kholas, Z. Eksp. i Teor. Fiz **61**, 2429 (1971) [Sov.

Phys. -JETP **34**, 1300 (1972)].

[37] J. Hammerberg and N. W. Ashcroft, Phys. Rev. B/bf 9, 409 (1974).

[38] H. Nagara, H. Miyagi, and T. Nakamura, Prog. Theor. Phys. **64**, 731 (1980).

[39] B. I. Min, H. J. F. Jansen, and A. J. Freeman, Phys. Rev. B**30**, 5076 (1984).

[40] H. Miyagi, T. Hatano, and H. Ngara, J. Phys. Soc. Jpn, **57**, 2751 (1988).

[41] J. Kohanoff *et al.*, Phys. Rev. Lett. **78**, 2783 (1997). ;J. Kohanoff, Proceedings of the Adriatico Research Conference: Simple Systems at High Pressures and Temperatures: Theory and Experiment, ICTP Science Abstract No 23, http://www.ictp.trieste.it/ pub_off/sci-abs/smr999 (ICTP, Trieste, October 1997).

[42] See for example, S. Ichimaru, Rev. Mod. Phys. **54**, 1017 (1982), and references therein.

[43] H. Nagara, J. Phys. Soc. Jpn, **58**, 3861 (1989).

[44] R. M. Hazen, H. K. Mao, L. W. Finger, and R. J. Hemley, Phys. Rev. B**36**, 3944 (1987).

[45] H. K. Mao *et al.* Science **239**, 1131 (1988)

[46] I. F. Silvera and R. J. Wijngaarden, Phys. Rev. Lett. **47**, 39 (1981).

[47] H. E. Lorenzana, I. F. Silvera, and K. A. Goettel, Phys. Rev. Lett. **64**, 1939 (1990).

[48] R. J. Hemley, H. K. Mao, and J. F. Shu, Phys. Rev. Lett. **65**, 2670 (1990).

[49] S. Tsuneyuki private communication.

[50] K. Nagao and H. Nagara, Phys. Rev. Lett. **80**, 548 (1998). The word "megabar" (Mbar) has been misprinted in the paper as "mbar".

[51] B. Edwards, N. W. Ashcroft, and T. Lenosky, Europhys. Lett. **34**, 519 (1996).

[52] J. S. Tse and D. D. Klug, Nature **378**, 595(1995).

[53] J. H. Eggert, H. K. Mao, and R. J. Hemley, Phys. Rev. Lett. **70**, 2301 (1993); M. I. M.

Scheerboom and J. A. Schouten, Phys. Rev. B**53**, R14705 (1996).

[54] See standard texts of the group theory, for example, *Symmetry Principles in Solid State and Molecular Physics* by M. Lax (Wiley-Interscience, New York, 1974).

[55] M. Hanfland, Phys. Rev. Lett. **69**, 1129 (1992).

[56] D. M. Ceperley and B. J. Alder, Phys. Rev B**36**, 2092 (1987); for recent quantum Monte-Carlo calculation see, for example, Ref. [35].

[57] R. D. King-Smith and R. J. Needs, J. Phys. Condens. Matter **2**,3431(1990) ;K. Karch, P. Pavone, W. Windl, O. Schütt, and D. Strauch, Phys. Rev. B **50**, 17054 (1994) ;O. Schütt, P. Pavone, W. Windl, K. Karch, and D. Strauch, Phys. Rev B **50**, 3746 (1994)

[58] R. Resta, in *Festkörperprobleme:Advance in Solid State Physics*, edited by P. Grosse (Viewer, Braunschweig,1985),Vol. 25, p.183, and references therein.

[59] M. C. Payne, M. P. Teter, D. C. Allen, T. A. Arias, and J. D. Joannopoulos, Rev. Mod. Phys. **64**, 1045 (1992)

[60] C. Elaässer, M. Fähnle, C. T. Chan, and K. M. Ho, Phys. Rev. B **49**, 13975 (1994).

[61] K. Nagao, T. Takezawa, and H. Nagara, to be published.

[62] K. Parlinski,Z. Q. Li, and Y. Kawazoe, Phys. Rev. Lett. **78**, 4063 (1997).

[63] Reason for the imaginary values of some "intepolated" frequencies is not clear. The possible stabilities near the Γ-point will be checked by the calculations of the elastic constants.

[64] Yu. Kagan, V. V. Pushkarev, and A. Kholas, Z. Eksp. Teor. Fiz /bf 73, 967 (1977) [Sov. Phys. -JETP /bf 46, 511 (1977).

[65] H. J. Jodl, W. Loewen, and D. Griffith, Solid State Commun, **61**, 8 (1987).

[66] D. Marx and M. Parrinello, Z. Phys. **95**, 143 (1994); J. Chem. Phys. **104**, 4077 (1996).

[67] T. Miyake, T. Ogitsu, and S. Tsuneyuki, Phys. Rev. Lett. **81**,1873 (1998).